LA-UR-02-7167
Approved for public release;
distribution is unlimited.

Title: **Gamma-ray production cross sections from neutron interactions with iron**

Author(s): R. O. Nelson, C. M. Laymon, S. A. Wender, D. M. Drake, M. Drosg S. G. Bobias, P. Englert, C. A. McGrath and C. V. McIsaac

Submitted to:

http://lib-www.lanl.gov/cgi-bin/getfile?00937016.pdf

Gamma-ray production cross sections from neutron interactions with iron

R. O. Nelson, C. M. Laymon*, S. A. Wender
LANSCE-3, Los Alamos National Laboratory, Los Alamos, NM 87545

D. M. Drake
Techsource Inc. and LANSCE-3, LANL, Los Alamos, NM 87545

M. Drosg
Institute for Experimental Physics, University of Vienna, A1090 Vienna, Austria

S. G. Bobias† and P. Englert‡
San Jose State University, San Jose, CA 95192

C. A. McGrath and C. V. McIsaac
Idaho National Engineering and Environmental Laboratory, Idaho Falls, ID 83415

Introduction

The initial purpose of this experiment was to provide a consistent data base of neutron-induced gamma-ray production cross sections over a large energy range for use in estimating elemental composition of the martian surface by observing gamma rays produced by cosmic ray interactions on the planet's surface [Bo02]. However, these data should be useful for other projects such as oil-well logging, accelerator transmutation of nuclear waste, shielding calculations, gamma-ray heating for nuclear reactors and verification of nuclear model calculations and databases.

The goal of the measurements was to collect data on the strongest gamma rays from many samples of interest. Because of the available beam time this meant that many of the measurements were rather short. Despite the short running time the large samples used and the good beam intensity resulted in very satisfactory results. The samples, chosen mainly as common constituents of rock and soil and measured in the same few week period, include: B_4C, BN, C, Al, Mg, Si, S, Ca, Ti, Cr, Mn, and Fe. Be was also used as a neutron scatterer that only produces one gamma ray (478 keV from ^{7}Li) with appreciable intensity. Thus Be can serve as a measure of neutron-induced backgrounds. In this first paper we present results for Fe.

There have been many measurements of neutron production of discrete gamma rays from iron nuclei, which have results that have been rather inconsistent. For example one can see these variations in comprehensive evaluations by S. P. Simakov *et al.* [Si98], and M. V. Savin *et al.* [Sa99]. The cross section for production of the 846.8-keV gamma ray from ^{56}Fe is considered a "standard" at the 10% level, yet at E_n = 14 MeV the recent evaluations by Simakov [Si98] and Savin [Sa99] differ by about 25%.

---

* Present address: University of Washington, Radiology Dept., Seattle, WA 98195-6004
† Present address: unknown
‡ Present address: University of Hawaii, Manoa, HI 96822

Similar photon production data have been acquired by Dickens *et al.* [Di90] at ORNL for some of the nuclei of interest using isotopically-enriched samples. However for the purpose of employing gamma rays to deduce the elemental composition of a planetary surface, it is advantageous to have cross sections for photon production from naturally occurring (i.e. elemental) isotopic mixtures. Our data also include cross sections for higher energy gamma rays than observed by Dickens *et al.* [Di90] where no gamma rays were reported above $E_\gamma = 2.3$ MeV.

Experimental Arrangement

The experiment reported here was carried out at the WNR facility of Los Alamos National Laboratory where a white source of neutrons is produced by bombarding a tungsten target with the 800 MeV pulsed proton beam from the LANSCE accelerator [Li90]. Neutrons from this target are collimated and used at various experiment stations. The station for this experiment was located 18.71 meters from the tungsten neutron production target, 15 degrees to the right of the direction of the proton beam. The neutron beam was well collimated with a rectangular spot size that was 8.89 cm wide and 9.31 cm high as measured with a small plastic scintillator on a scanning stage.

The proton beam pulse width at the target was less than 1 ns. Separation time between proton pulses was 1.8 μs. The neutron flux as a function of time was measured during gamma-ray data accumulation by a fission ion chamber that contained thin (~400 $\mu g/cm^2$) deposits of both ^{238}U and ^{235}U [We93]. The fission chamber was located 15.498 m from the neutron production target.

The neutron energy was deduced from the time difference between the arrival of the proton pulse at the tungsten target and the detection of a neutron-induced gamma ray in the germanium detector. Similarly the energy of a neutron at the fission chamber was deduced from the difference between the time of occurrence of a fission event and the time of the proton pulse on the tungsten target, accounting for the different flight path length of the fission chamber.

The sample was a natural iron disk 0.617-cm thick and 12.725 cm diameter, weighing 607.9 g, with chemical purity of 99.9%, oriented at 45 degrees with respect to the neutron beam. The iron disk was obtained from Cerac Inc. (Lot 33759A).

A schematic diagram of the experimental setup is shown in Fig. 1. A 97 cm^3 high purity Ge gamma-ray detector was located approximately 73 cm from the sample at 125 degrees relative to the neutron beam. In order to reduce the neutron-induced background in the detector, a 4.8-cm thick cylinder of ^6LiD was placed in front of the detector.

The efficiency of the counter was measured using a set of Amersham reference sources, a calibrated ^{152}Eu source and a ^{56}Co source. A calculated efficiency using a Monte Carlo code was in good agreement with the measurements. The efficiency contains the factor 4π so that the cross sections are for total production (neglecting angular distribution effects). Due to its lower acceptance and hence poorer statistics, the data from the 90-degree detector have not been analyzed.

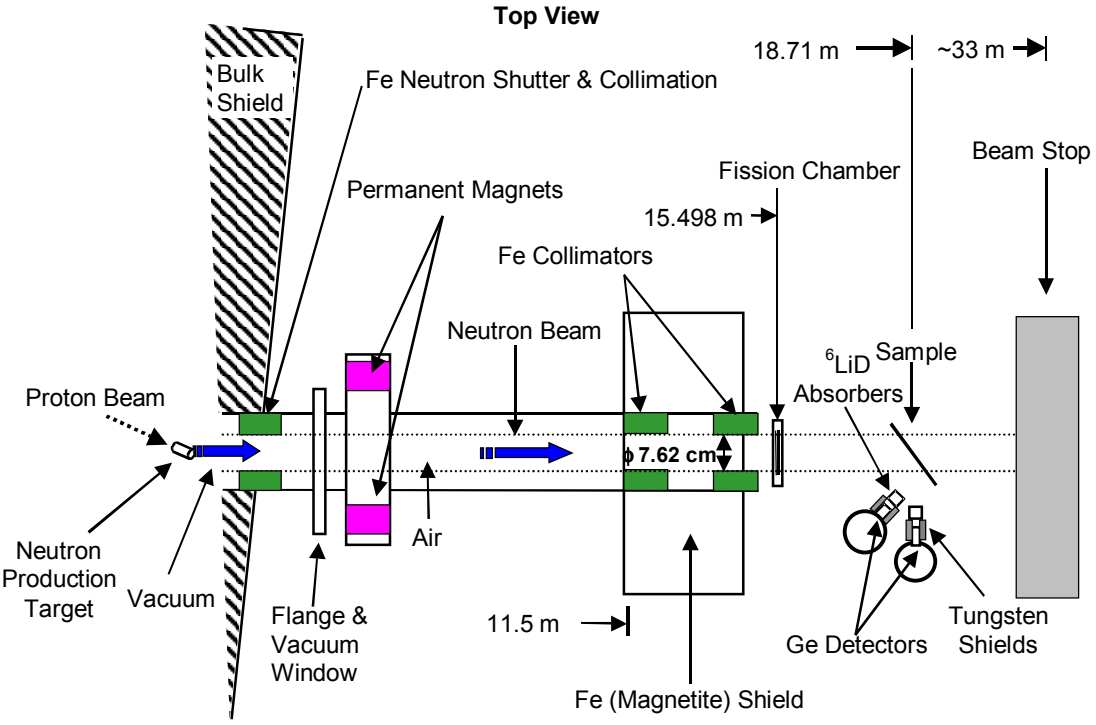

Fig. 1. Top-view schematic diagram of the experimental setup showing the neutron production target, collimation, fission chamber, sample and detectors. The distances indicated with arrows are measured from the neutron production target. The drawing is not to scale.

The spectroscopy amplifier, fast amplifier and CFD were located in the experimental shed near the Ge dectectors. The amplified signals were then sent to a data acquisition trailer where they were gated, digitized, and stored on a computer. A common power system was used to minimize ground loops and noise. The data acquisition system used the Indiana University version of XSYS [Yo81] in which data were recorded in event-by-event mode on a MicroVAX computer. For the Ge detectors, LeCroy Research Systems (LRS) 3512 ADCs coupled to LRS 4302 CAMAC memory modules were used to record the pulse height and Ortec time-to-amplitude converters (TACs) connected to LRS 3512 ADCs provided the timing information. The time spectra were calibrated using an Ortec time calibrator. The fission chamber time spectra and pulse height spectra were both recorded using a Silena model 4418 8-channel ADC and Ortec TACs. All data were buffered in fast memory during beam macropulses and read out via CAMAC between macropulses to reduce the dead time.

Slow-risetime rejection was used in the Ortec model 473A constant fraction discriminators to improve the detector timing, but with a reduction in efficiency at low pulse heights. A block diagram of the electronics is given in Fig. 2. A Tennelec TC 203A amplifier was used with a shaping time constant of 1 μs for the pulse height. This time constant setting kept pileup effects from degrading the gamma-ray energy resolution, while allowing fairly high counting rates. The instantaneous count rate in the detectors during a macropulse was kept at or below about 10 k counts/s.

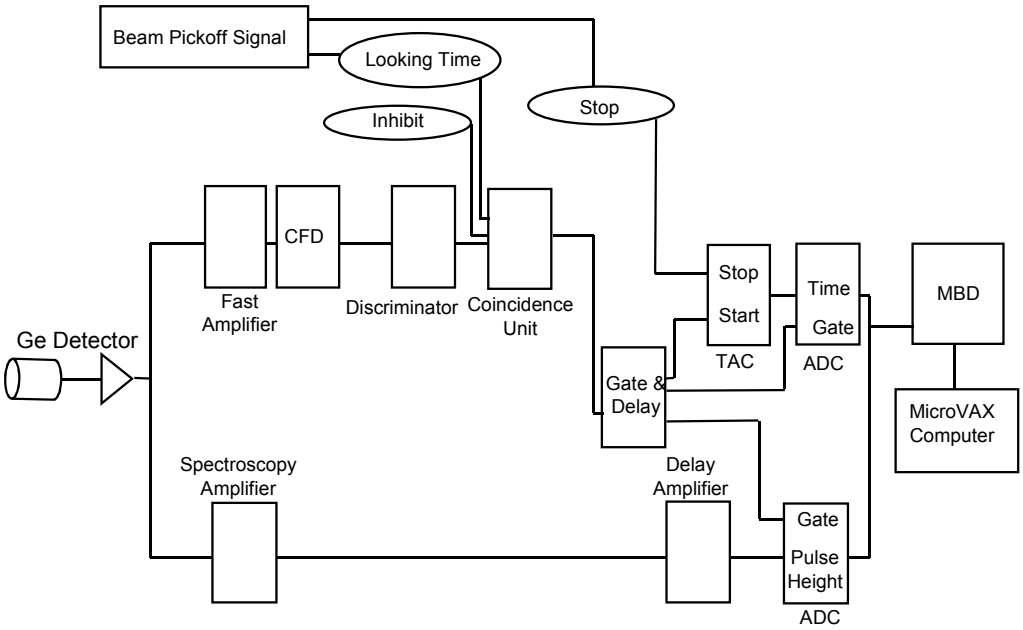

Fig. 2 Block diagram of the data acquisition electronics showing the main pulse height and time-of-flight branches. The fast amplifier and constant fraction discriminator (CFD) and spectroscopy amplifier were located near the Ge detector, while the other electronics and computer were in a remote trailer. The proton beam pickoff signal was generated well before the neutron production target.

Data Reduction and Analysis

The low-energy gamma-ray time-of-flight data were corrected for the reduced efficiency through the measured efficiencies. The observed time walk as a function of pulse height was determined from the gamma flash (from the neutron production target) and a correction was made to the time spectra. Corrections for acquisition dead time (~4% and 8%) for the fission and germanium counters were also made. Data from both the fission chambers and the gamma-ray detector were binned so that the energy bin widths progressed from 0.2 MeV at 1 MeV to 5 MeV at 100 MeV. The neutron fluences deduced from the fission data are shown in Fig. 3. The structure is the result of the energy binning.

Corrections for neutron attenuation, multiple scattering, and gamma attenuation in the sample were made for each analyzed gamma ray for neutron energies from 1 to 20 MeV by the Monte Carlo code, MCNPX [Wa99]. Calculations were made for two samples, one of which had a density of one tenth that of the true sample. The correction made in this way accounts for neutron reactions that remove neutrons from the initial beam, neutrons that have scattered or produced other neutrons and can cause additional gamma-ray producing reactions, and gamma-ray attenuation probability. Above a neutron energy of 20 MeV, the cross-section library does not contain gamma-ray production data so corrections were made using estimates of neutron production, average path length and cross sections for the secondary neutrons. These corrections tend to be

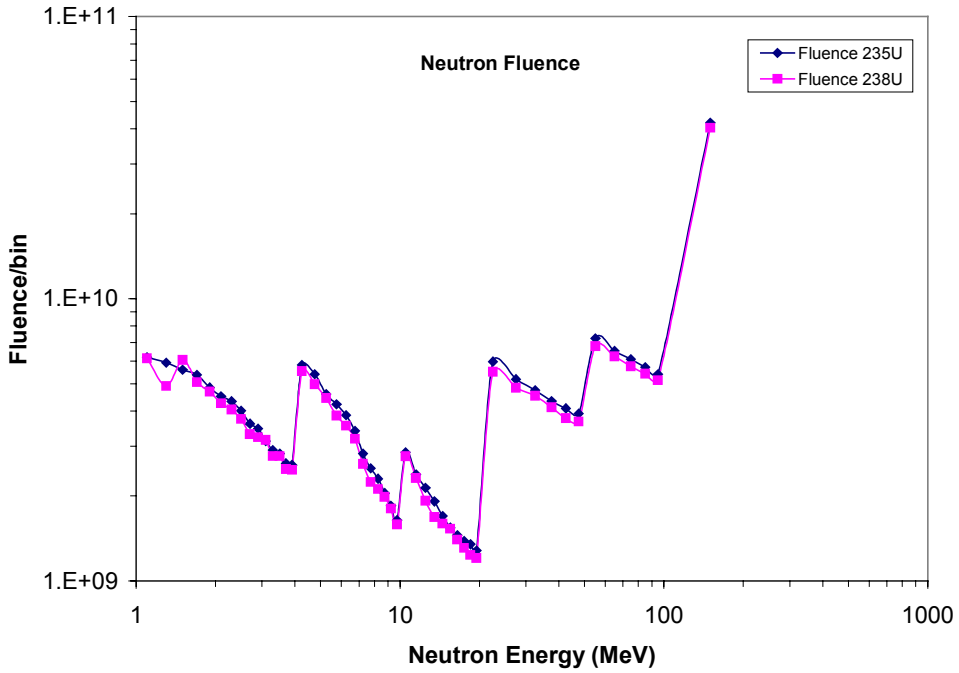

Fig. 3. Total neutron fluence as measured with the ^{235}U and ^{238}U foils of the fission chamber. The step-like structure is due to the chosen neutron-energy bin sizes.

large and less reliable. However this technique applied to the data below 20 MeV agree well with the MCNPX calculations.

For production of gamma rays that require high neutron energies the multiple scattering effect is lower and some cross sections reported here extend to neutron energies above 20 MeV.

Areas of the gamma-ray peaks were extracted using the XSYS analysis program and divided by the corresponding efficiency, neutron fluence and areal density of the sample. The above scattering and attenuation corrections were applied to obtain corrected cross sections. Peaks that were not clearly distinguished from background were not processed resulting in graphs that end or begin abruptly. Gamma rays with energies below 840 keV were not analyzed due to the greater attenuation in the relatively thick sample and the larger backgrounds at lower gamma-ray energies.

Backgrounds from long-lived sources were searched for in the data below the reaction thresholds. No significant background lines were seen. Even the ^{56}Fe(n, p)^{56}Mn –> ^{56}Fe* beta decay, that populates (either directly or via cascades) the 846.8-kev state in ^{56}Fe ~99% of the time, was not observed to be a problem in this measurement due to the low production of ^{56}Mn and the short time gating used. The half-life of this beta decay is 2.5789 h.

Due to the Fe disk being rotated 45 degrees with respect to the beam, some of the neutron beam did not strike the sample. Thus a correction for the solid angle of the sample with respect to the beam was required. This correction resulted in a 9% increase in the cross sections.

The neutron fluence was determined from the fission chamber data using the ENDF/B-VI [We91] evaluated cross sections for ^{238}U(n, f) and ^{235}U(n, f) for E_n < 16

MeV and the data of Lisowski *et al.* [Li91] for higher energies. The fission foil thicknesses were calculated from the mass of the deposit (from the manufacturer, Isotope Products Lab. Inc.) divided by the area. The fission chamber deposits are larger than the beam spot so that the entire fluence is measured, and these deposits appear to have good uniformity based on visual inspection.

Results

With an iron sample of natural isotopic composition, often reactions on more than one isotope can contribute to the production of a particular gamma ray. The contribution to the gamma-ray intensity from an isotope will be in proportion to the abundance of that isotope and the cross section for the reaction. For natural iron the abundances are: ^{54}Fe – 5.845%, ^{56}Fe - 91.754%, ^{57}Fe – 2.119%, ^{58}Fe – 0.282%. Different reactions have different energy thresholds, thus whether a particular reaction contributes to the gamma-ray production depends on whether its threshold has been exceeded. Reactions products observed and production thresholds are given in Table 1 [Ma97] where E_{level} includes a kinematic factor (=57/56 for inelastic scattering).

Table 1 – Thresholds for γ-Ray Production (MeV) [Ma97]

Sample/Product	^{56}Fe	^{55}Fe	^{54}Fe	^{52}Cr
^{54}Fe			E_{level}	7.83946+E_{level}
^{56}Fe	E_{level}	11.39934+E_{level}	20.865+E_{level}	7.75047+E_{level}
^{57}Fe	7.78155+E_{level}	19.17733+E_{level}	28.64005+E_{level}	15.5296+E_{level}
^{58}Fe	17.99863+E_{level}	29.391+E_{level}	38.85088+E_{level}	25.74437+E_{level}

In three cases (931.3+935.5, 1408.1+1408.4, 1670.8+1668 keV) gamma rays from different product nuclei were not separated, and we report the sums.

Figures 4, 5 and 6 show examples of the gamma-ray spectra for three different

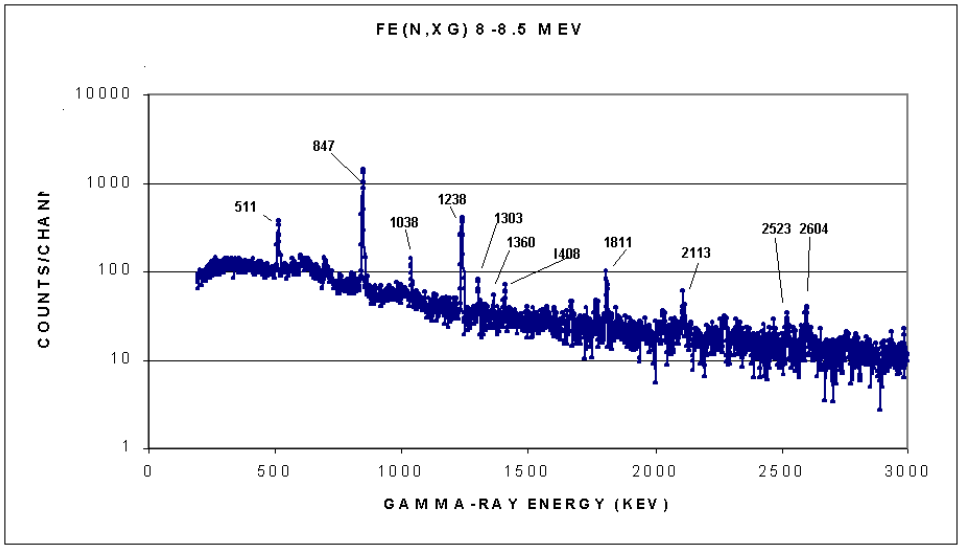

Fig. 4. Gamma-ray spectrum produced by neutrons in the energy range 8 to 8.5 MeV. Energies of some gamma-rays are indicated above the peaks in keV.

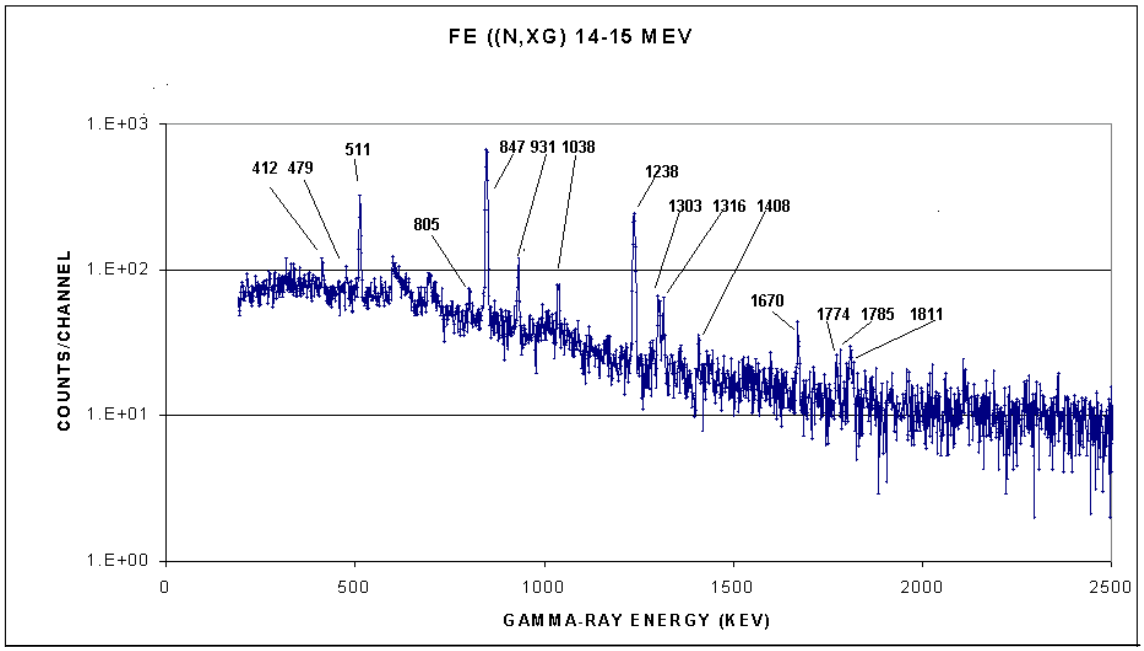

Fig. 5. Gamma-ray spectrum produced by neutrons in the energy range 14 to 15 MeV. Energies of some gamma-rays are indicated above the peaks in keV.

neutron energy regions. Energies of prominent peaks are indicated in the figures. The level schemes of the reaction products reported here (^{56}Fe, ^{55}Fe, ^{54}Fe, and ^{52}Cr) are given in Figs. 7 – 14 for reference purposes.

Cross sections for 16 gamma rays produced by inelastic excitation of ^{56}Fe are reported here. The excitation of the first 10 excited states of ^{56}Fe as well as the 12th, 17th, 19th, 21st, 23rd, and 24th levels was observed. A few strong gamma rays from the (n,2n), (n,3n) and (n,na) reactions on ^{56}Fe are also given. In many cases minor contributions from reactions on the less abundant Fe isotopes are present. The ^{54}Fe(n,n') reaction exciting the first 2^+ level in ^{54}Fe is the strongest of these reactions. The cross sections reported are for twenty gamma-ray energies. They are presented both as figures 15 through 34 and in Tables 2.- 21. All cross sections are given for natural iron [isotopic ^{56}Fe cross sections would be 1/91.7% (=1.09) times greater].

Where possible the data are plotted with the results of Dickens *et al.* [Di90] (reduced by a factor of 0.92 to convert to "natural" Fe cross sections) and with the evaluations of Simakov *et al.* [Si98] and Savin *et al*. [Sa99]. It is important to note that Dickens experiment [Di90] used an isotopically enriched ^{56}Fe sample and thus, in many cases, may differ somewhat from our results due to the addition of usually small contributions from reactions on the other isotopes in our sample (5.845% ^{54}Fe, 2.119% ^{57}Fe, and 0.282% ^{58}Fe). In general, good agreement of the excitation function shapes is observed, but in some energy regions and for some gamma rays, larger normalization differences are seen.

For a few gamma rays we get very different results from Dickens *et al.* (see E_γ = 1669.9, 1434, 2034.8 and 2094.9. keV, for examples). The cause of such differences is not known, although we would argue that our excitation functions exhibit the behavior expected from nuclear model calculations. As examples preliminary GNASH calculations are shown in Figs. 22, 23, 25, and 26.

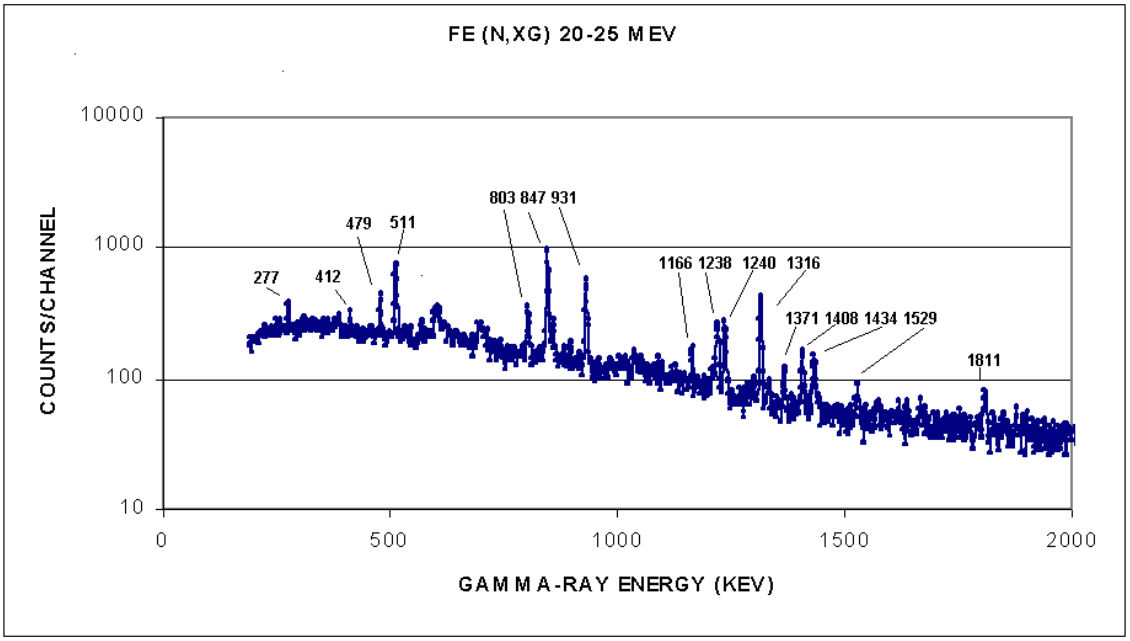

Fig. 6. Gamma-ray spectrum produced by neutrons in the energy range 20 to 25 MeV. Energies of some gamma-rays are indicated above the peaks in keV.

Because many measurements (at least 22 [Si98]) have been made on iron near 14.5 MeV neutron energy, the cross sections for gamma rays at this energy are often used as a standard to which one compares. In this tradition, the cross section reported here for the 847-keV gamma ray at 14.5 MeV is 663 +/-70 mb, while the evaluations of Savin *et al*. [Sa99] and of Simakov *et al*. [Si98] are 621 +/- <62 and 785 +/- 48 mb respectively. For the 1238-keV gamma ray, the results are: present 305 +/- 33 mb, [Sa99] 277 +/- <41 mb and [Si98] 393 +/- 22 mb. For the 1811 keV gamma ray: 51 +/- 8 mb, [Sa99] 44 mb and [Si98] 63 +/- 5 mb. Our results appear to be intermediate between the two evaluations at 14.5 MeV. Savin *et al.* describe the 847-keV evaluation as accurate to 5 to 10%, the 1238-keV evaluation as accurate to 10 to 15 % and are less certain of the accuracy of the 1811-keV line.

Summary

Spectra of gamma rays produced by the interaction of neutrons from 1 to 150 MeV at the LANSCE-WNR white source have been collected and analyzed to produce cross sections. Several of the prominent gamma rays can be compared to previous measurements. Because there are large variations in previous measurements, it is not surprising that our measurements do not agree with some. However our measurements do agree quite well with much of the data of Dickens *et al.* [Di90], and our results are intermediate between the evaluations Simakov [Si98] and Savin [Sa99]. In addition, because the spectra were taken in one experiment the ratios of gamma-ray production cross sections should be free of major systematic errors. Corrections for multiple scattering, made using Monte Carlo techniques, become large for high-energy neutrons and gamma rays with low thresholds. Data for six higher-energy gamma rays are given

here for the first time and some excitation functions have been extended to much higher energies than previously available.

Acknowledgments

The authors would like to thank R. C. Reedy for discussions and support. This work was supported by the US DOE at Los Alamos National Laboratory under contract number W-4705-ENG-36, by the National Aeronautics and Space Administration under contract number Y712322, and by the US DOE Idaho Operations Office under contract DE-AC07-99ID13727.

References

[Bo02] W.V. Boynton, W. C. Feldman, S. W. Squyres, T. H. Prettyman, J. Bruckner, L. G. Evans, R. C. Reedy, R. Starr, J. R. Arnold, D. M. Drake, P. A. J. Englert, A. E. Metzger, Igor Mitrofanov, J. I. Trombka, C. d'Uston, H. Wanke, O. Gasnault, D. K. Hamara, D. M. Janes, R. L. Marcialis, S. Maurice, I. Mikheeva, G. J. Taylor, R. Tokar, and C. Shinohara, "Distribution of Hydrogen in the Near Surface of Mars: Evidence for Subsurface Ice Deposits", Science **297**, 81-85 (2002).

[Ch99] Figures produced by Isotope Explorer v. 2.23 (1999), S. Y. Chu, *et al*. available at the world wide web site: http://ie.lbl.gov/isoexpl/isoexpl.htm , using data from the ENSDF database which is a compilation of the work of many authors available at the National Nuclear Data Center world wide web site: http://www.nndc.bnl.gov/ensdf/.

[Di90] J. K. Dickens, *et al.*, International Conference on Nuclear Data for Science and Technology, Juelich, Germany, 1991, and Oak Ridge National Laboratory Technical Report, ORNL-TM-11671, 1990.

[Li90] P. W. Lisowski, C. D. Bowman, G. J. Russell, and S. A. Wender, "The Los Alamos National Laboratory Spallation-Neutron Sources," Nucl. Sci. Eng. **106**, 208 (1990).

[Li91] Fission Cross Section Ratios for ^{233,234,236,238}U Relative to ^{235}U from 0.5 to 400 MeV, P.W. Lisowski, A. Gavron, W.E. Parker, A.D. Carlson, O.A. Wasson, N.W. Hill, Proceedings of the International Conference on Nuclear Data for Science and Technology, Juelich, Germany, 13-17 May, 1991, p 732.

[Ma97] R. MacFarlane *et al.*, QTOOL, (1997); Available at the world wide web site: http://t2.lanl.gov/data/qtool.html.

[Sa99] M. V. Savin, A. V. Livke and A. G. Zvenigorodskij, "Evaluation of Angular Distributions and Production Cross-Sections for Discrete Gamma Lines in Iron," INDC (CCP) 426 p. 95 (2000) translated from Yadernye Konstanty 2 (1999). Available at the world wide web site: http://iaeand.iaea.or.at/indc_sel.html.

[Si98] S.P. Simakov, A. Pavlik, H. Vonach, and S. Hlavac, "Status of Experimental and Evaluated Discrete γ-Ray Production at En=14.5 MeV," INDC(CCP)-413 (1998).

[Wa99] L. S. Waters, Ed., *MCNPX User's Guide*, Los Alamos National Laboratory Report, LA-UR-99-6058, (1999).

[We91] ENDF/B-VI evaluation of ^{238}U, by L. W. Weston *et al*., MOD 2, MAT 9237, Revision 1991; evaluation of ^{235}U, by L. C. Leal *et al*., MOD 2, MAT 9228, Revision 1991; data retrieved from the ENDF database (http://www.nndc.bnl.gov/).

[We93] S. A. Wender, S. Balestrini, A. Brown, R. C. Haight, C. M. Laymon, T. M. Lee, P. W. Lisowski, W. McCorkle, R. O. Nelson, and W. Parker, "A Fission Ionization Detector for Neutron Flux Measurements at a Spallation Source," Nucl. Instrum. Methods A **336**, 226 (1993).

[Yo81] N. R. Yoder, "XSYS, IUCF Data Acquisition Software," IUCF internal report 1991 and IEEE Trans. Nucl. Sci. **NS-28**, 3708, 3815, 3822, 3834 (1981).

[Yo92] Comprehensive Nuclear Model Calculations: Introduction to the Theory and Use of the GNASH Code, P. G. Young, E. D. Arthur, and M. B. Chadwick, Los Alamos National Laboratory report LA-12343-MS, 1992.

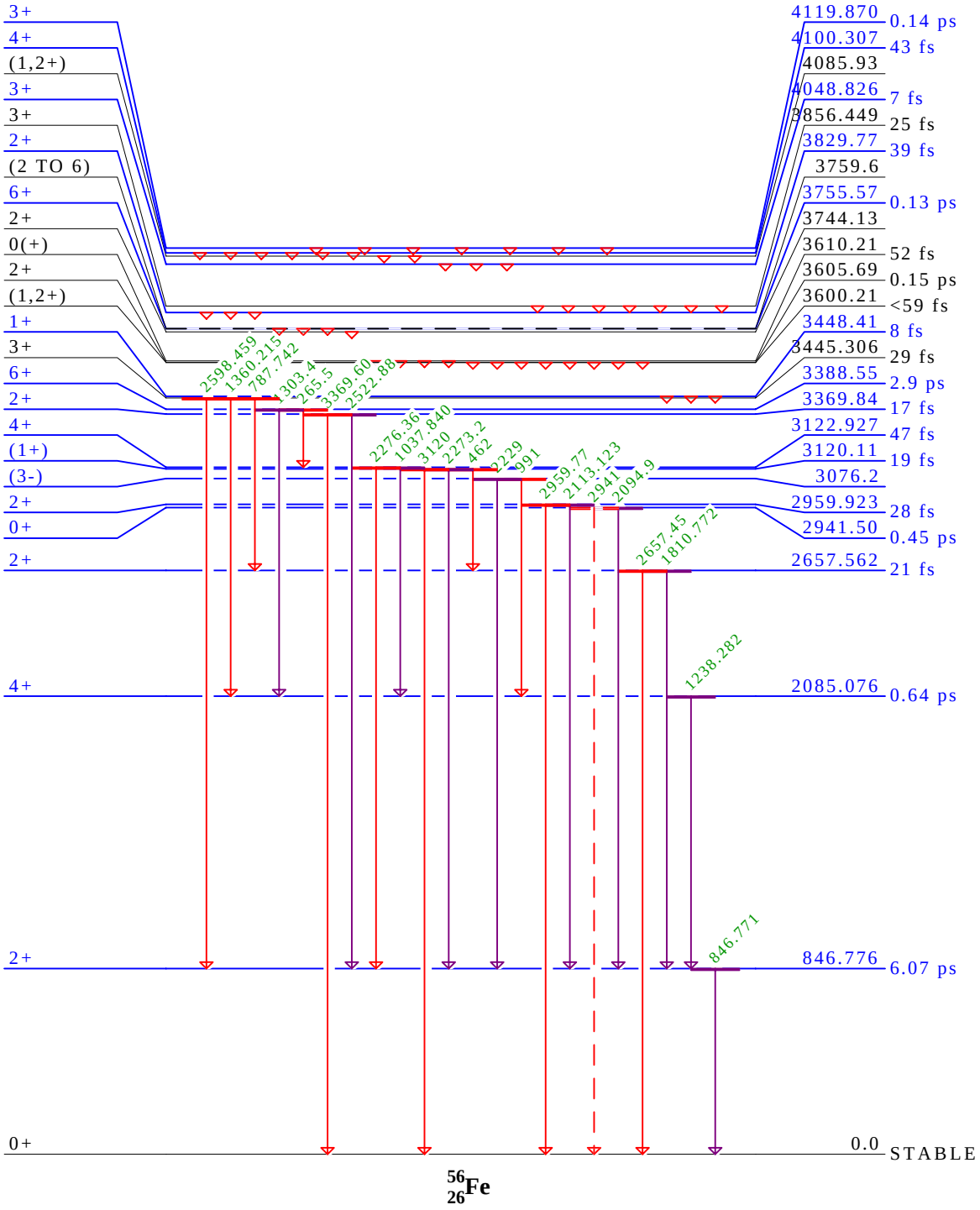

Fig. 7. Level diagram for ^{56}Fe produced by Isotope Explorer[Ch99]. Transitions were observed from levels shown in blue. Gamma-rays are shown for the lower levels here and for higher levels in Figs. 8, 9 and 10. Gamma-rays shown in purple were observed in our measurements.

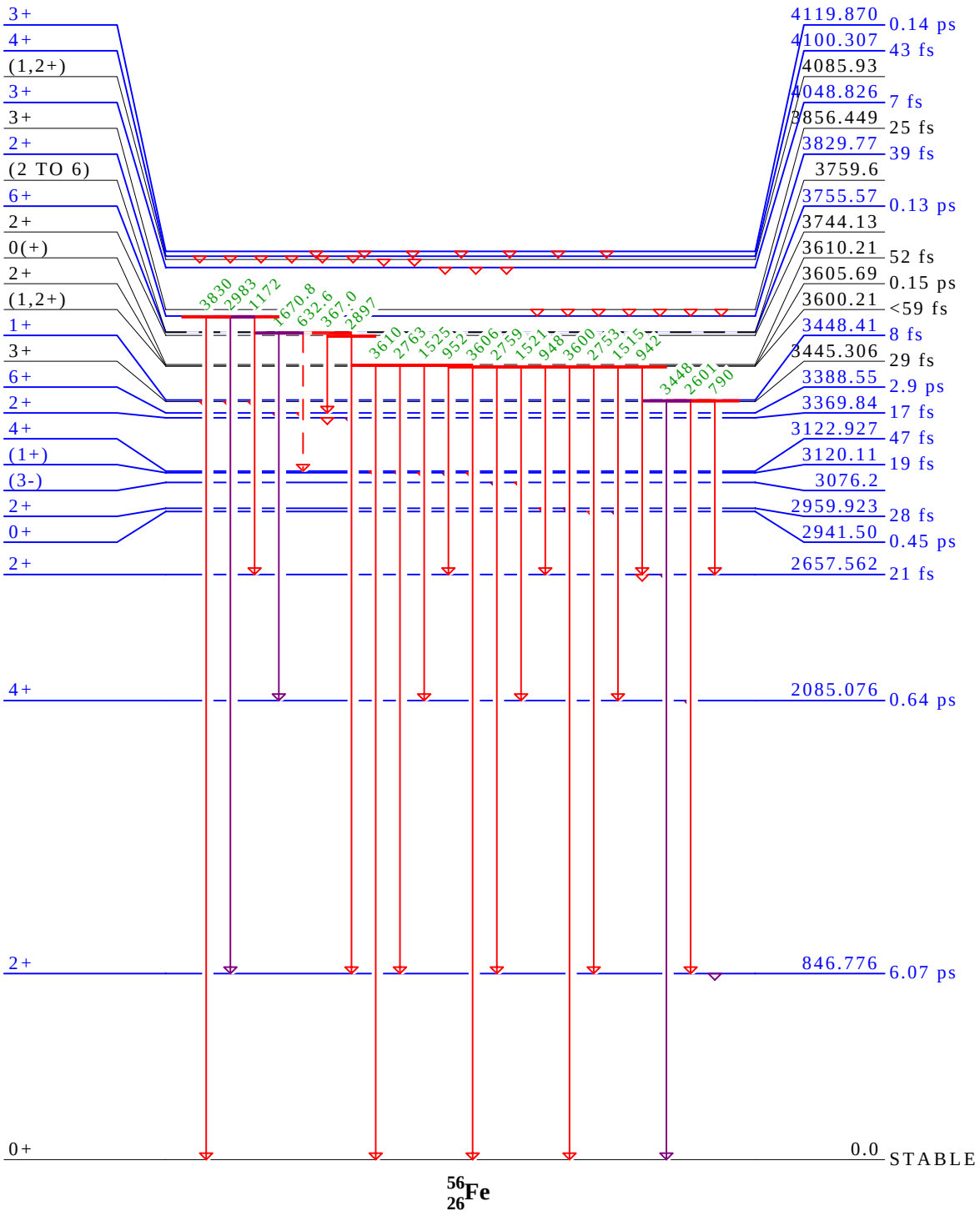

Fig. 8. Level diagram for ^{56}Fe produced by Isotope Explore [Ch99]. Transitions were observed from levels shown in blue. Gamma-rays are shown for intermediate levels here and for lower and higher levels in Figs. 7, 9 and 10. The gamma-rays shown in purple were observed in our measurements.

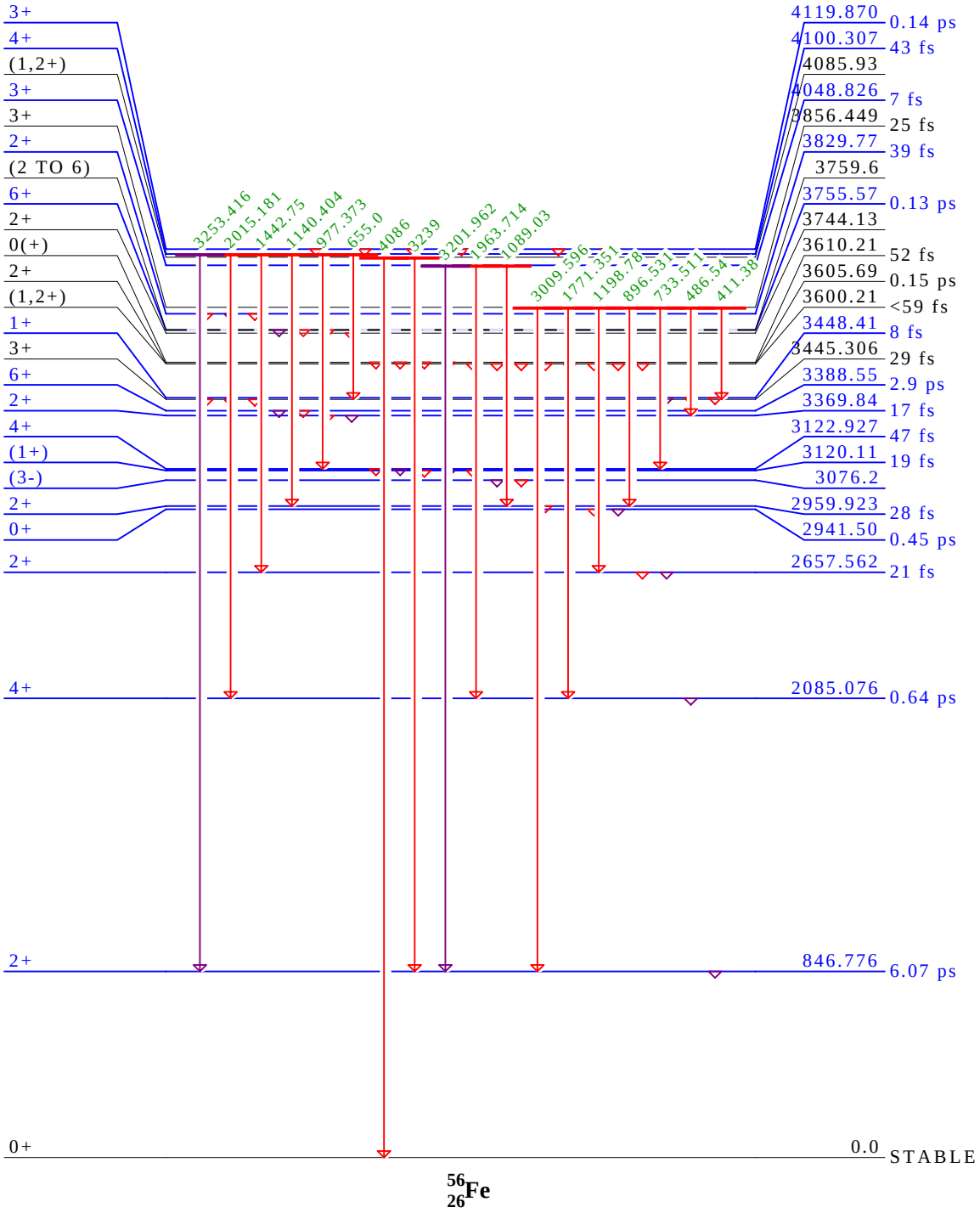

Fig. 9. Level diagram for ^{56}Fe produced by Isotope Explorer [Ch99]. Transitions were observed from levels shown in blue. Gamma-rays are shown for the higher levels here and in Fig. 10, and for lower levels in Figs. 7 and 8. The gamma-rays shown with purple arrows were observed in our measurements.

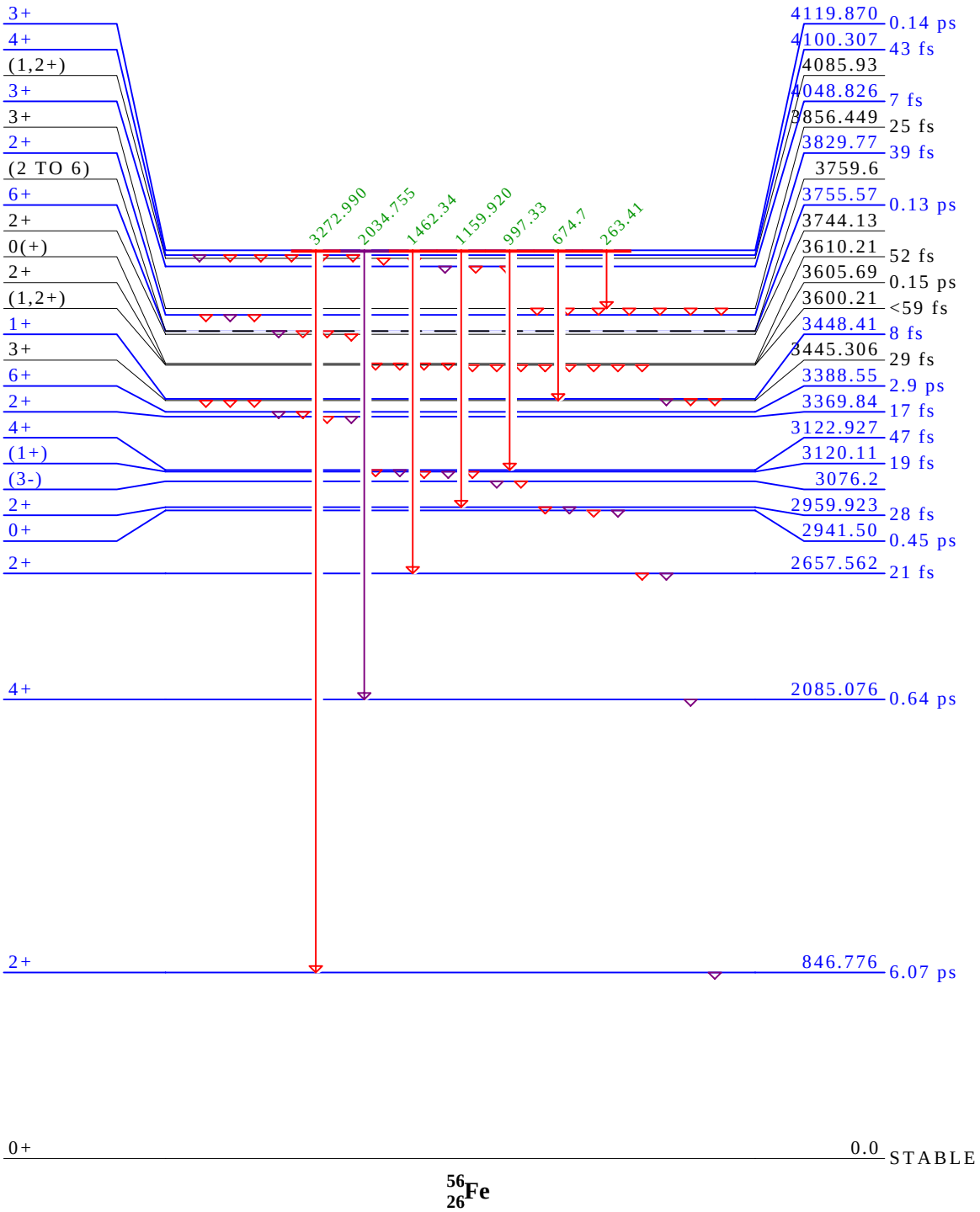

Fig. 10. Level diagram for ^{56}Fe produced by Isotope Explorer [Ch99]. Transitions were observed from levels shown in blue. Gamma-rays are shown for the highest observed levels here and for lower levels in Figs. 7, 8 and 9. The gamma-ray shown with a purple arrow was observed in the present measurements.

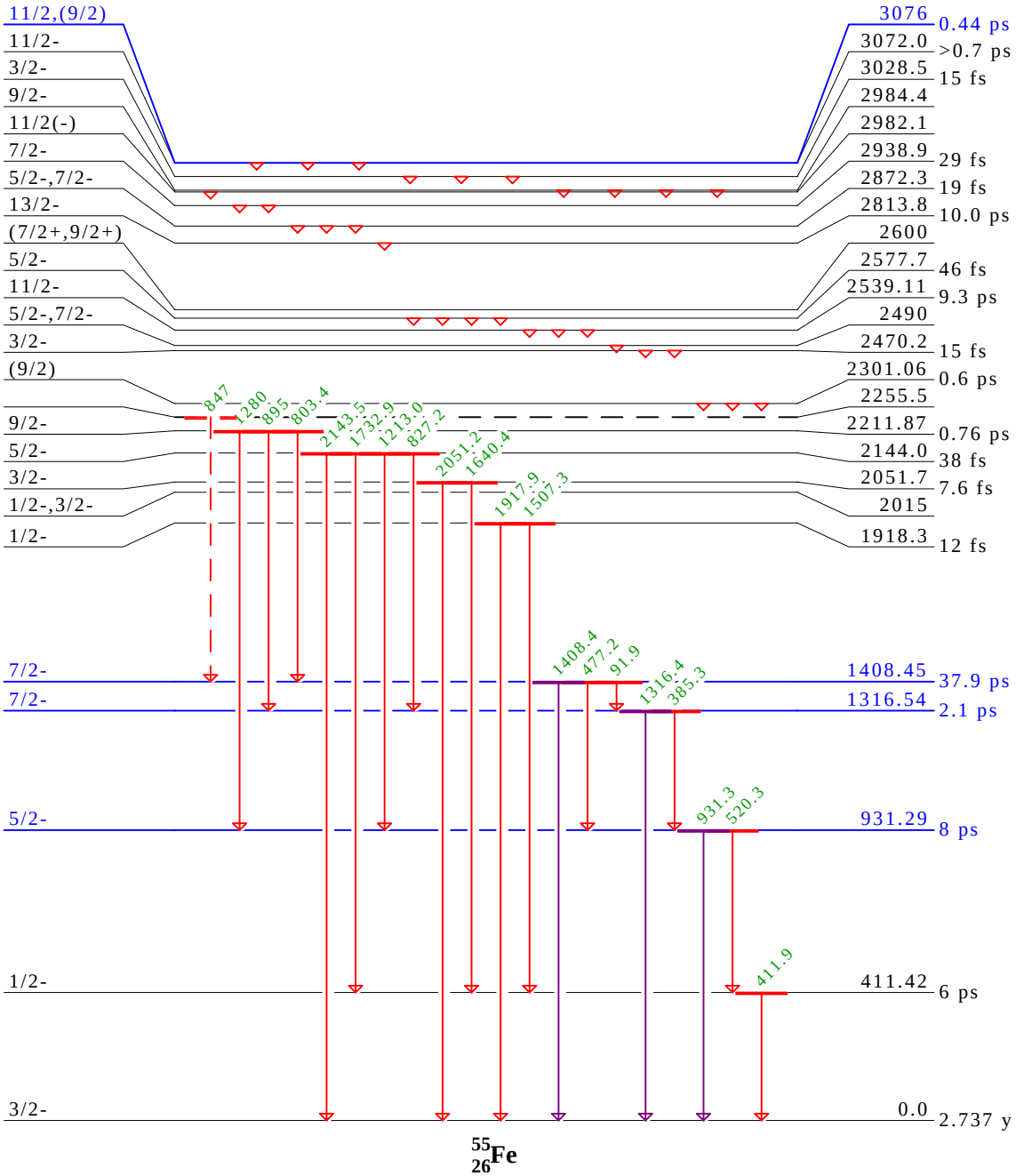

Fig. 11. Level diagram for ^{55}Fe produced by Isotope Explorer [Ch99]. Transitions were observed from levels shown in blue. Gamma-rays are shown for the lower levels here and for higher levels in Fig. 12. The gamma-rays shown by purple arrows were observed in our measurements.

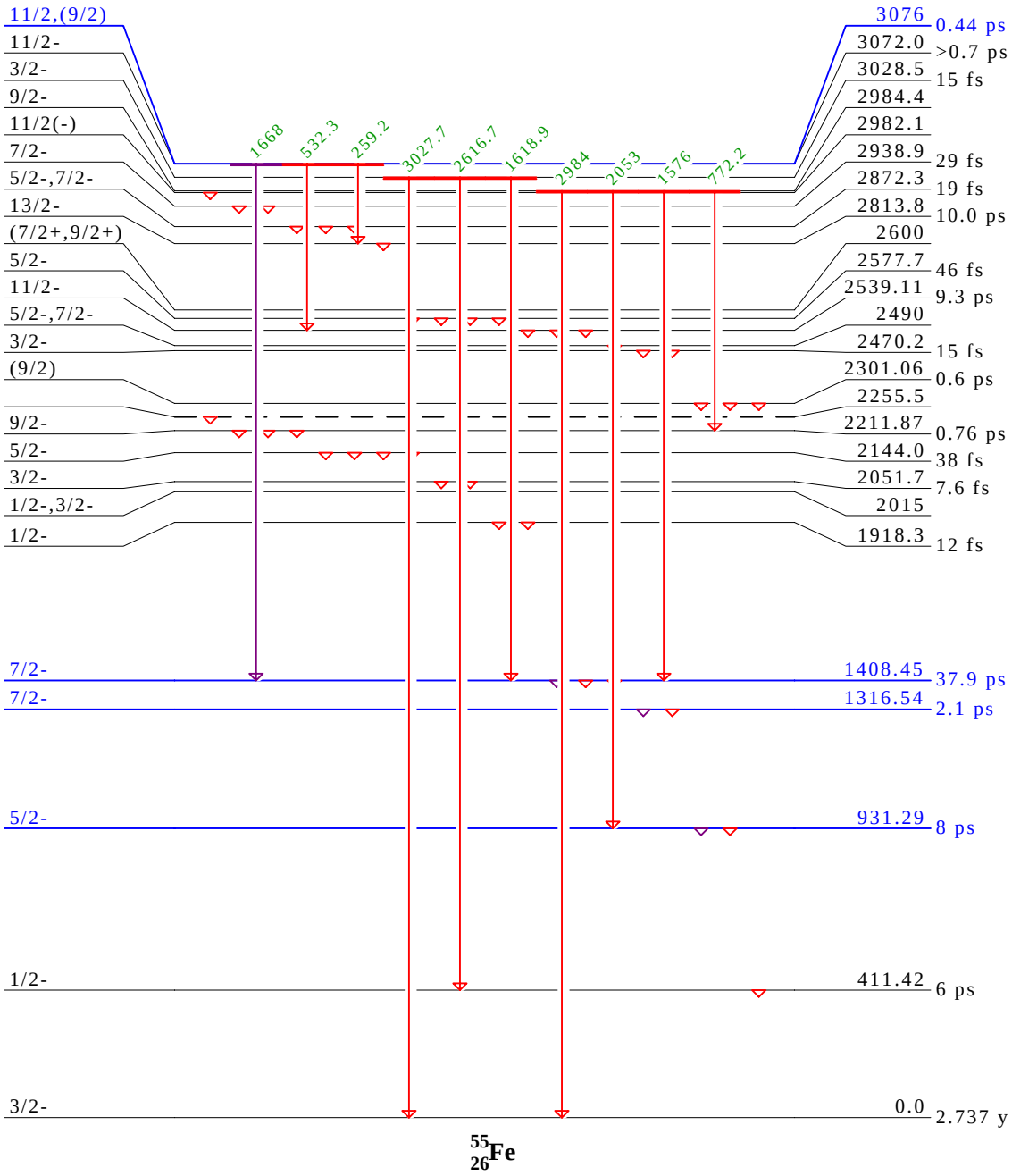

Fig. 12. Level diagram for ^{55}Fe produced by Isotope Explorer [Ch99]. Transitions were observed from levels shown in blue. Gamma-rays are shown for the higher levels here and for lower levels in Fig. 11. The gamma-rays shown by purple arrows were observed in the present measurements.

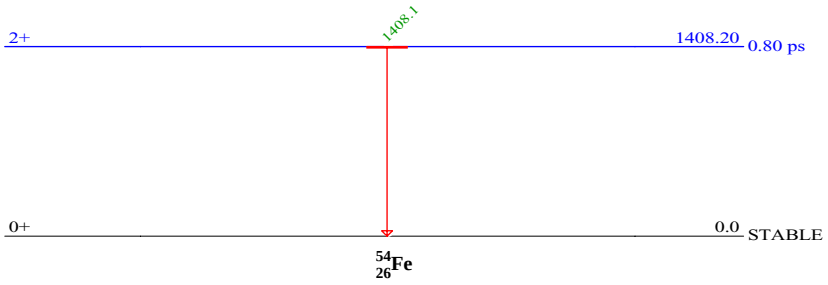

Fig. 13. Level diagram for ^{54}Fe produced by Isotope Explorer [Ch99]. Only the one transition shown was observed.

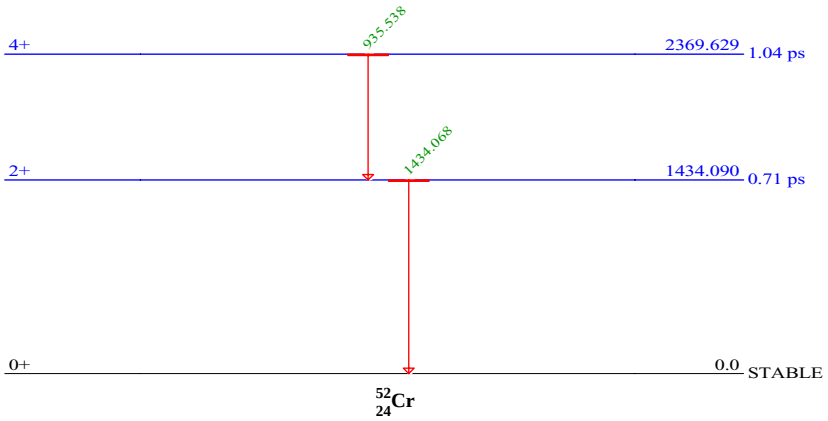

Fig. 14. Level diagram for ^{52}Cr produced by Isotope Explorer [Ch99]. Only the two transitions shown were observed.

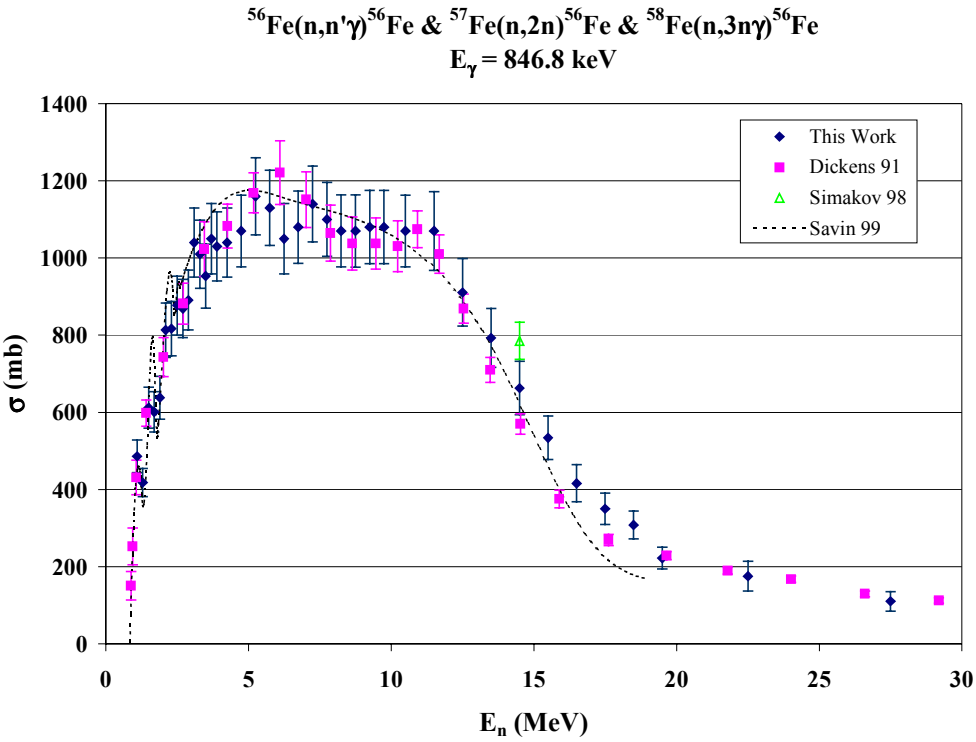

Fig. 15. Cross sections for the 846.8-keV gamma ray from the first excited state of ^{56}Fe. The data of Dickens *et al.* and the evaluations of Simakov *et al.* [Si98] and Savin *et al.* [Sa99] are shown for comparison. Agreement is better at lower energies and not good above 14 MeV.

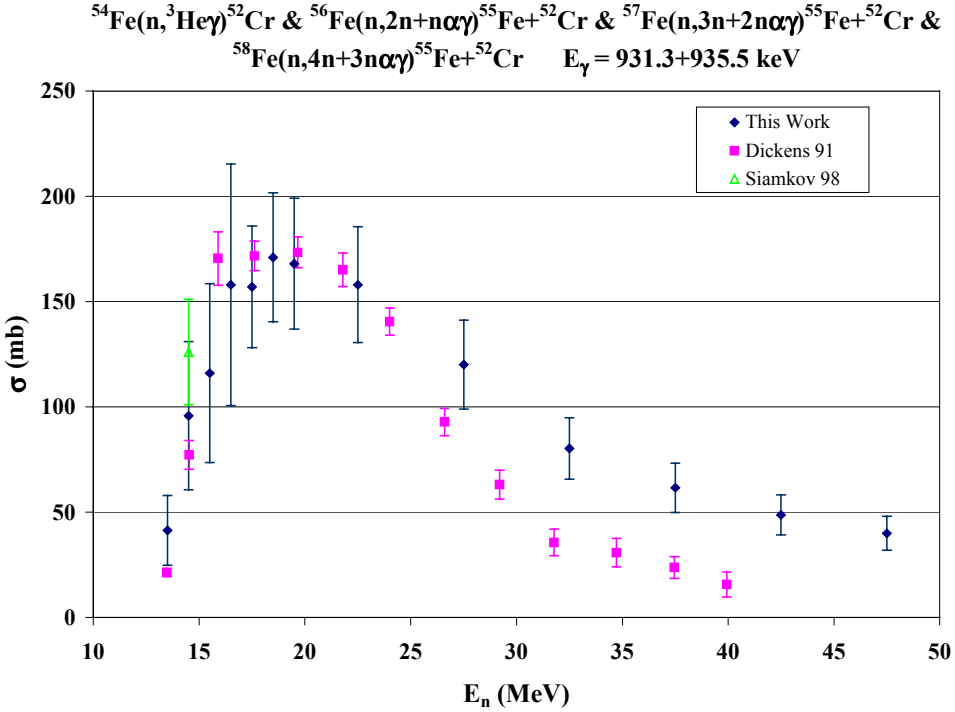

Fig. 16. Cross sections for the sum of the 931.3- and 935.5-keV gamma rays from the 2nd excited states of ^{52}Cr and ^{55}Fe. The thresholds are 12.3 and 10.2 MeV for ^{55}Fe and ^{52}Cr production, respectively. The data of Dickens *et al.* [Di90] and the evaluation of Simakov *et al.* [Si98] are shown for comparison.

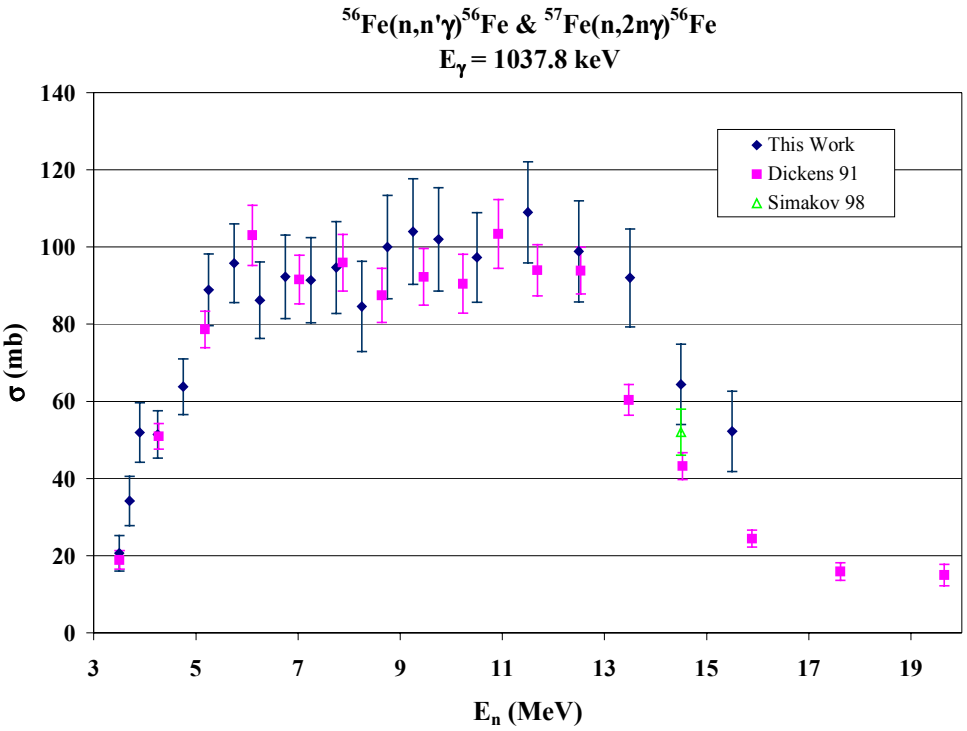

Fig. 17. Cross sections for the 1037.8-keV gamma ray from ^{56}Fe(n,n$_8$'γ). The data of Dickens *et al.* [Di90] and the evaluation of Simakov *et al.* [Si98] are shown for comparison.

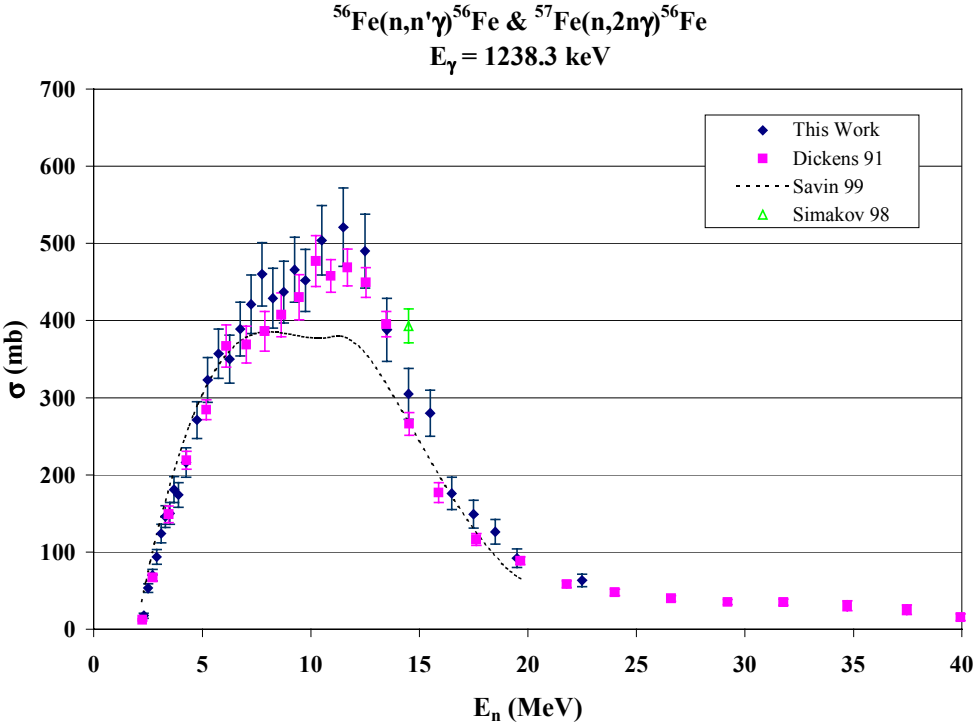

Fig. 18. Cross sections for the 1238.3-keV gamma ray from ^{56}Fe(n,n$_2$'γ). The data of Dickens *et al.* [Di90] and the evaluations of Simakov *et al.* [Si98] and Savin *et al.* [Sa99] are shown for comparison. We observe poor agreement with both evaluations.

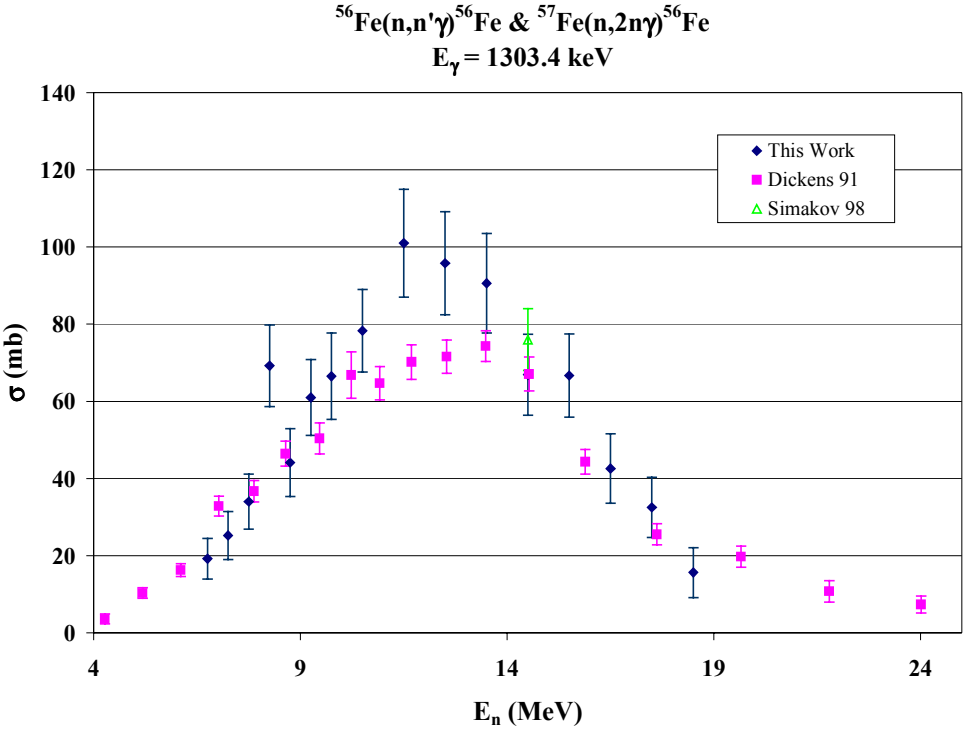

Fig. 19. Cross sections for the 1303.4-keV gamma ray from ^{56}Fe(n,n$_{10}$'g). The data of Dickens *et al.* [Di90] and the evaluation of Simakov *et al.* [Si98] are shown for comparison.

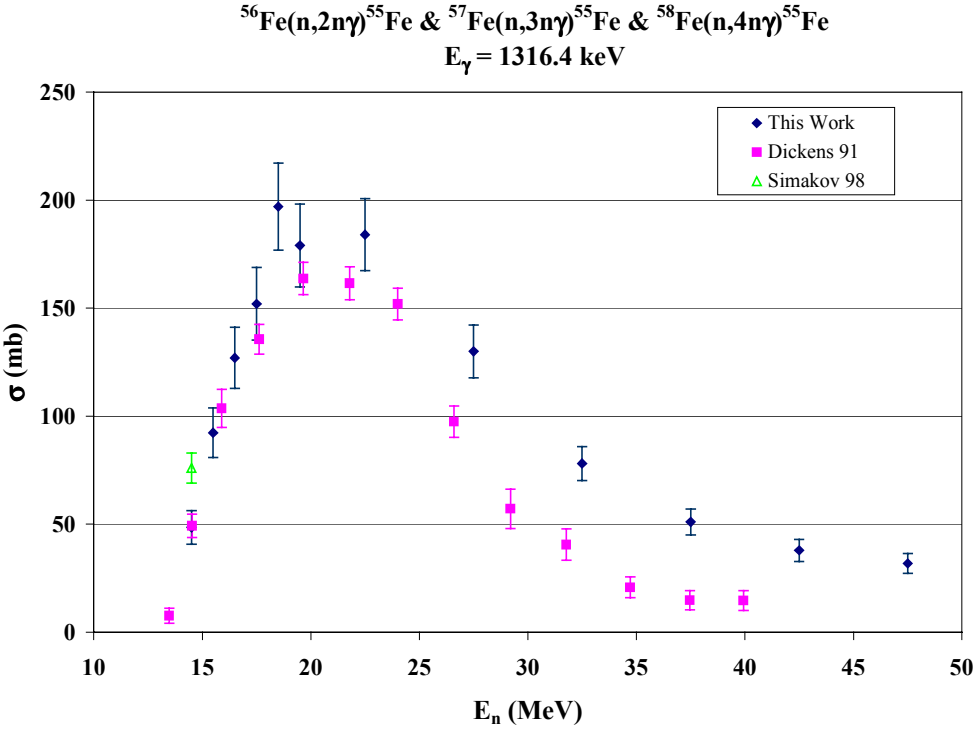

Fig. 20. Cross sections for the 1316.4-keV gamma ray from the 3rd excited state of ^{55}Fe with a threshold of 12.7 MeV. The data of Dickens *et al.* [Di90] and the evaluation of Simakov *et al.* [Si98] are shown for comparison.

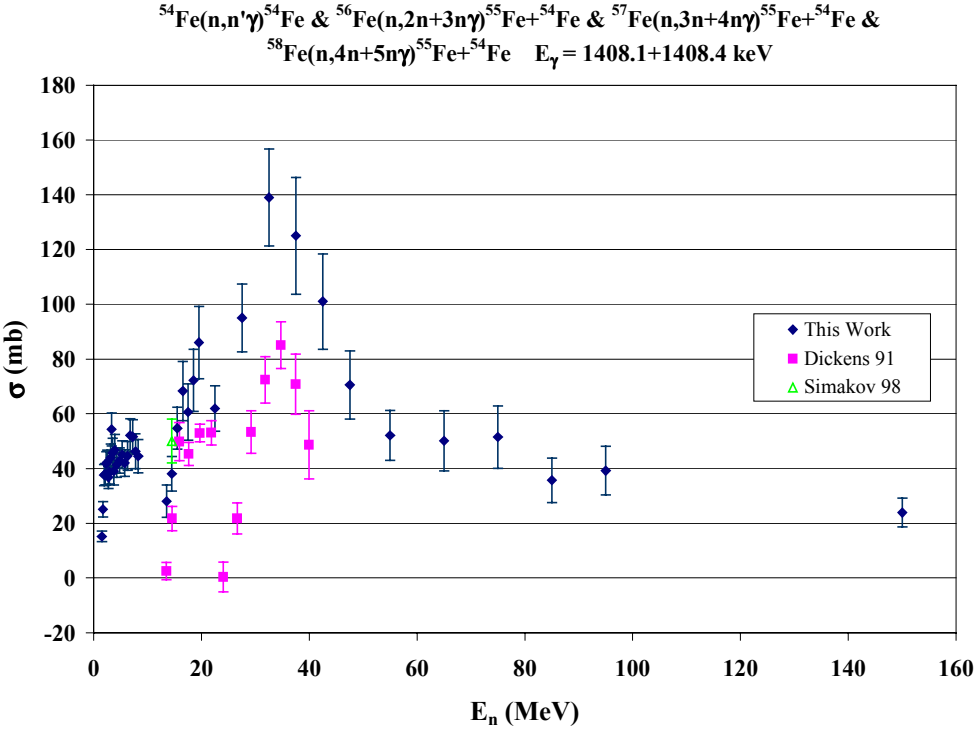

Fig. 21. Cross sections for the 1408.1-keV gamma ray from the 1st excited state of ^{54}Fe and the 1408.4-keV gamma ray from the 4th excited state of ^{55}Fe. The lower (1-10 MeV) portion is due to ^{54}Fe(n,n'γ) with a threshold of 1.43 MeV, while the higher-energy part is mostly from the ^{56}Fe(n,2nγ) and (n,3nγ) reactions The data of Dickens *et al.* [Di90] and the evaluation of Simakov *et al.* [Si98] are shown for comparison.

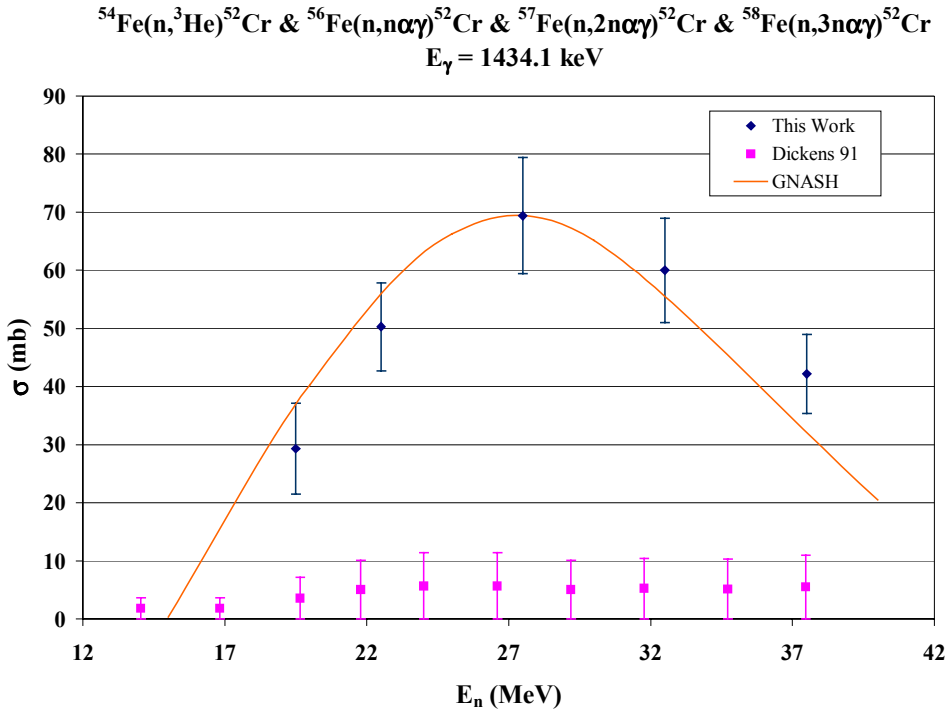

Fig. 22. Cross sections for the 1434.1-keV gamma ray from ^{56}Fe(n,nα$_1$γ)^{52}Cr with a threshold of about 9.2 MeV. The data of Dickens *et al.* [Di90] do not agree with our data, while preliminary GNASH [Yo92] nuclear reaction model calculations [Yo97] agree quite well.

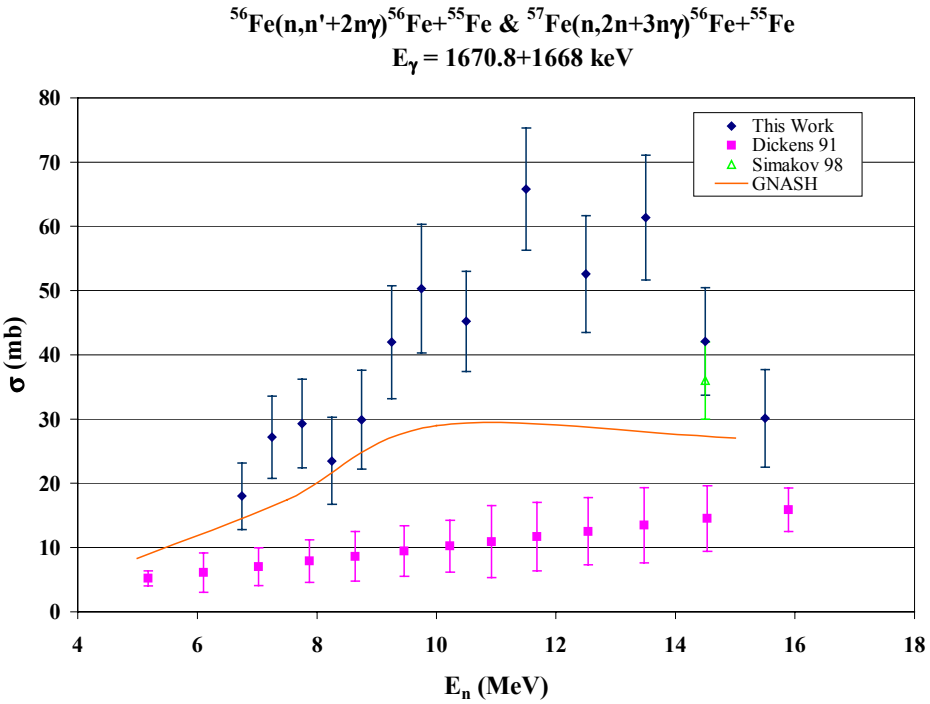

Fig. 23. Cross sections for the 1670.8-keV gamma ray from ^{56}Fe(n,n$_{17}$'γ) and the 1668-keV gamma ray from ^{55}Fe. There is no agreement with the data of Dickens *et al.* [Di90] while the evaluation of Simakov *et al.* [Si98] agrees within errors with our data. A preliminary GNASH [Yo92] calculation [Yo97] for the 1670.8-keV line shows similarity in shape to the lower part of our data. The 1668-keV line was not included in the calculation.

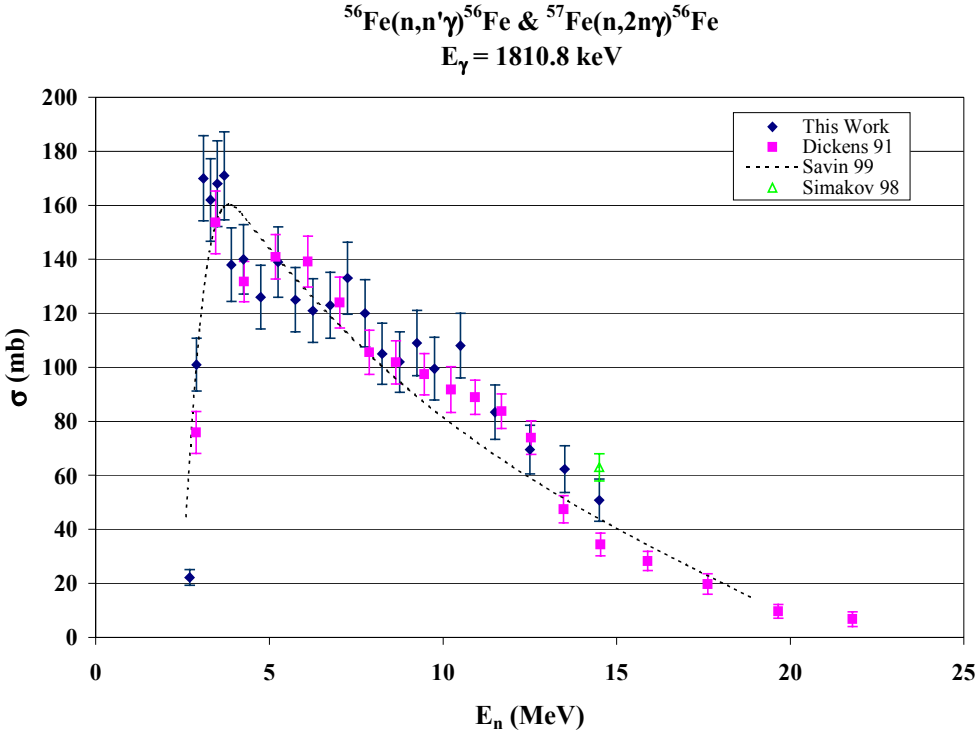

Fig. 24. Cross sections for the 1810.8-keV gamma ray from the 3rd excited state of ^{56}Fe. The data of Dickens *et al.* [Di90] and the evaluations of Simakov *et al.* [Si98] and Savin *et al.* [Sa99] are shown for comparison.

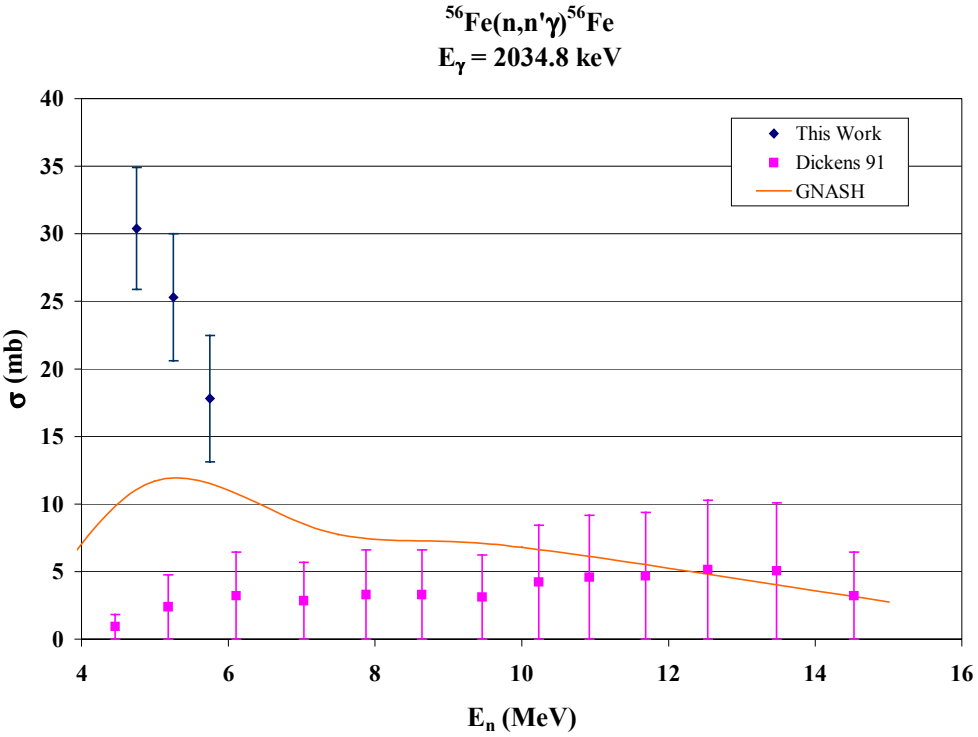

Fig. 25. Cross sections for the 2034.8-keV gamma ray from the ^{56}Fe(n,n$_{24}$'γ). The data of Dickens *et al.* [Di90] do not agree with the present results, which are supported by the shape of the curve of preliminary GNASH [Yo92] reaction model calculations [Yo97].

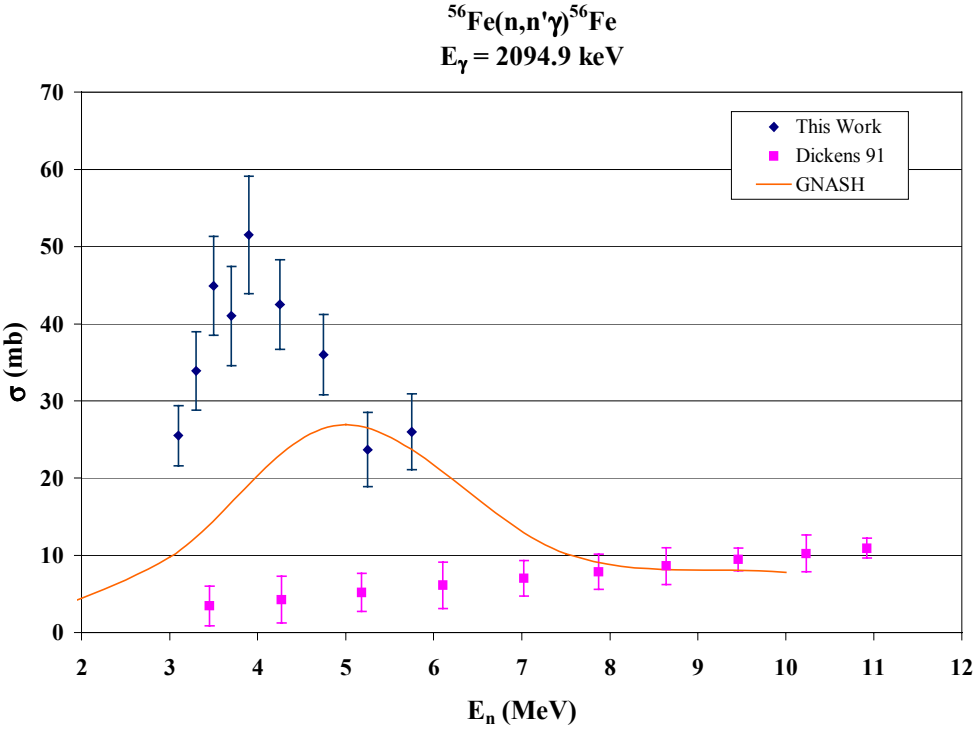

Fig. 26. Cross sections for the 2094.9-keV gamma ray from the ^{56}Fe(n,n$_4$'γ). The data of Dickens *et al.* [Di90] do not agree with the present results. The trend in the GNASH [Yo92] reaction model calculations [Yo97] is similar to our data.

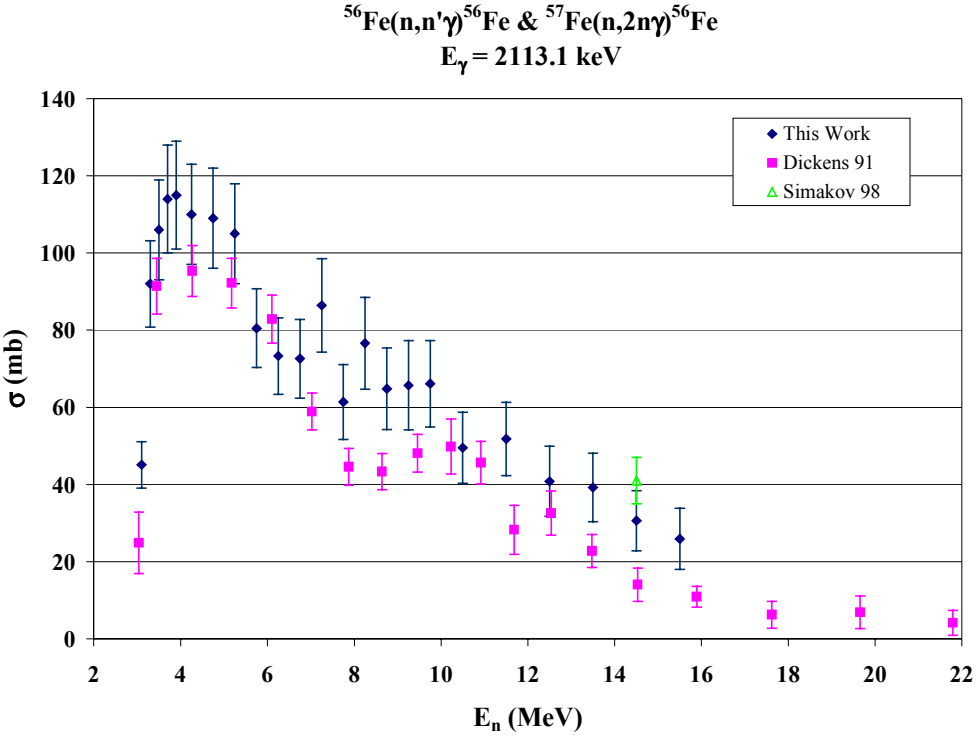

Fig. 27. Cross sections for 2113.1-keV gamma ray from the ^{56}Fe(n,n$_5$'γ). The data of Dickens *et al.* [Di90] and the evaluations of Simakov *et al.* [Si98] are shown for comparison.

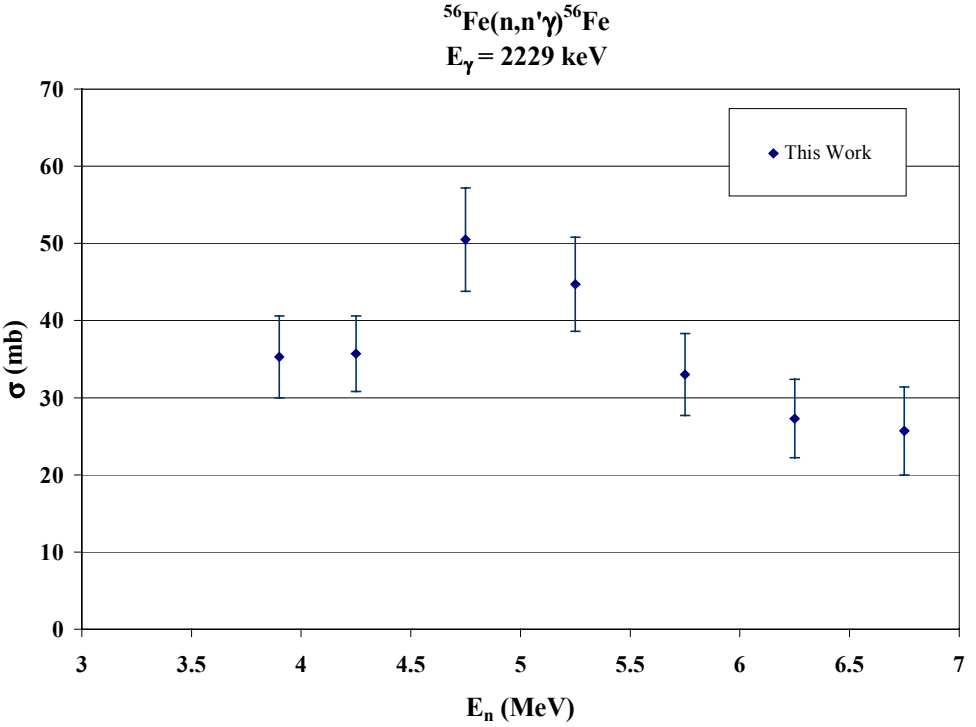

Fig. 28. Cross sections for the 2229-keV gamma ray from the ^{56}Fe(n,n$_6$'γ).

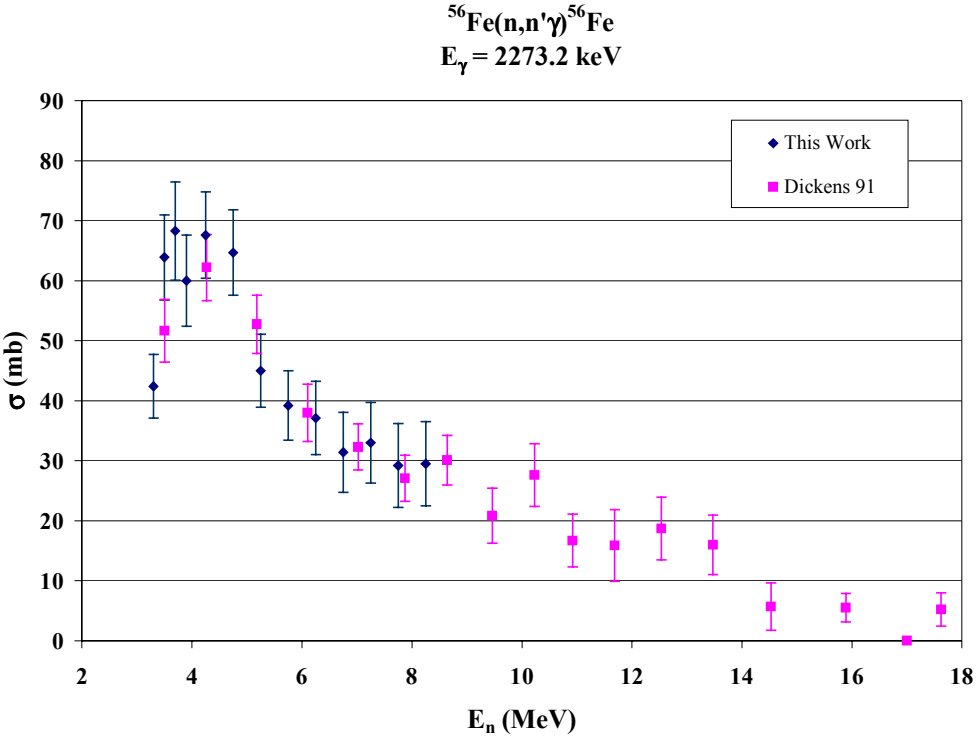

Fig. 29. Cross sections for the 2273.2-keV gamma ray from the ^{56}Fe(n,n$_7$'γ). The data of Dickens *et al.* [Di90] are shown for comparison.

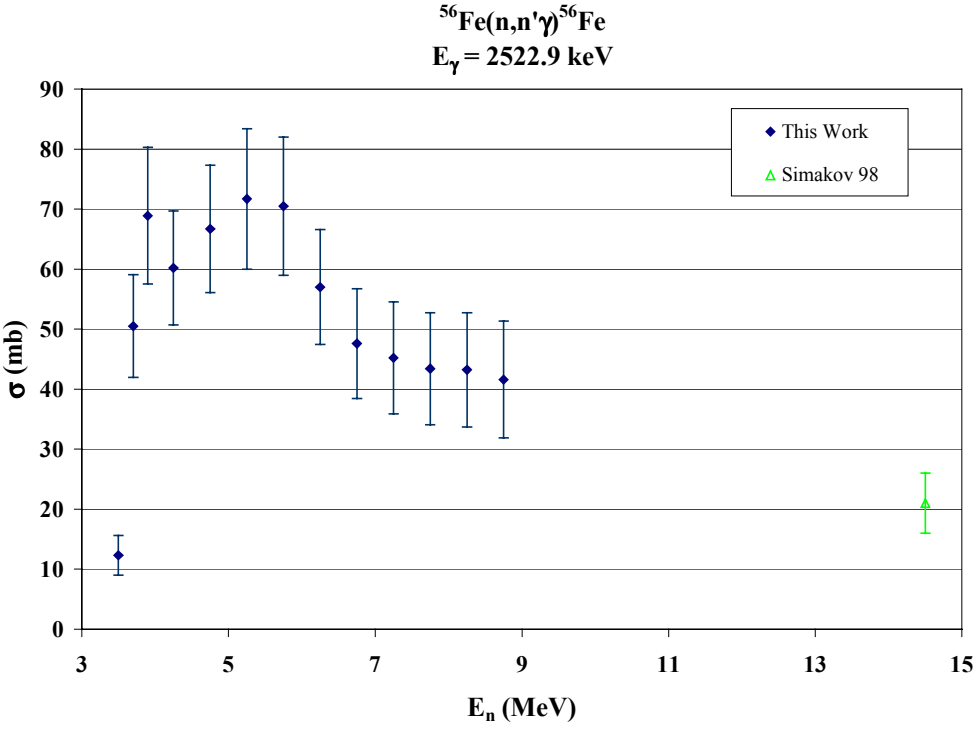

Fig. 30. Cross sections for the 2522.9-keV gamma ray from the ^{56}Fe(n,n$_9$'γ). The evaluation of Simakov *et al.* [Si98] is shown at E_n = 14.5 MeV.

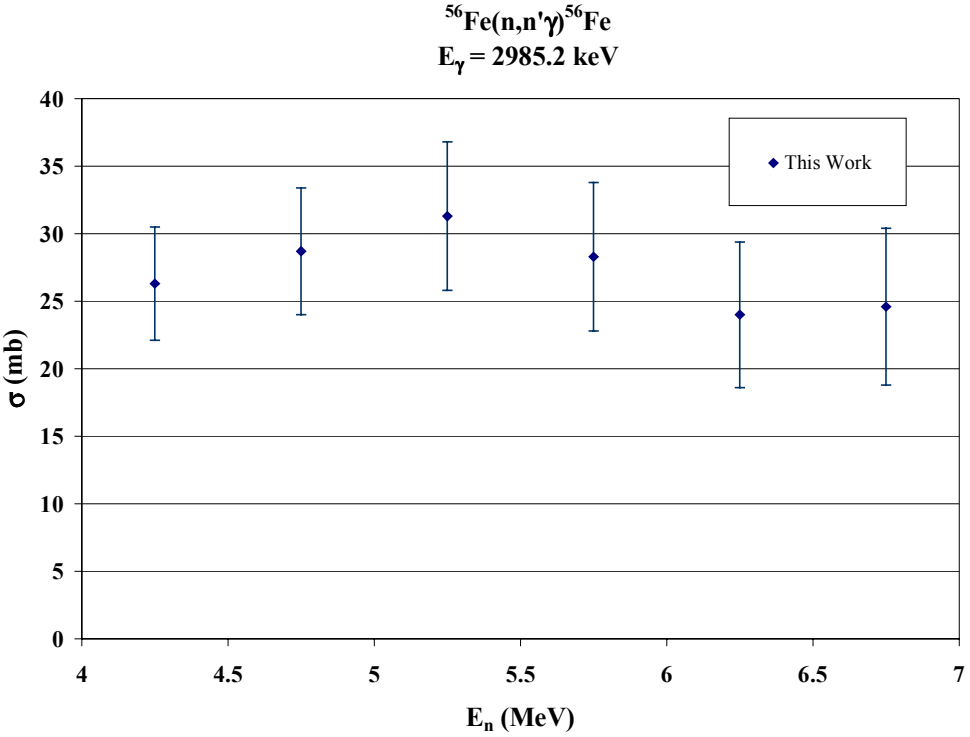

Fig. 31. Cross sections for the 2985.2-keV gamma ray from ^{56}Fe(n,n$_{19}$'γ).

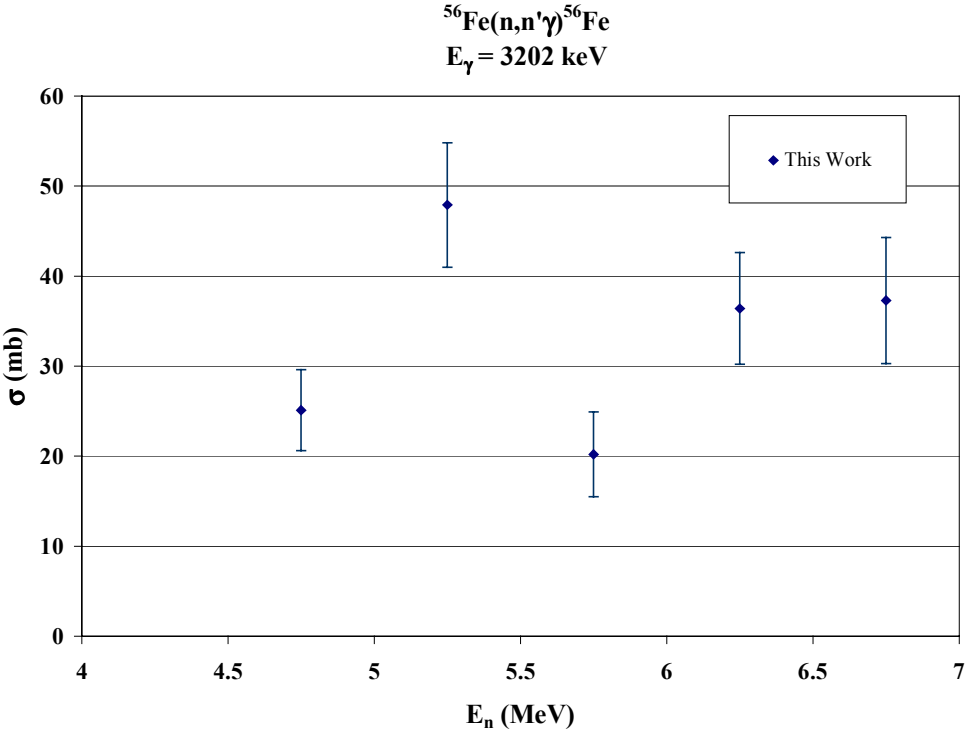

Fig. 32. Cross sections for the 3202-keV gamma ray from ^{56}Fe(n,n$_{21}$'γ).

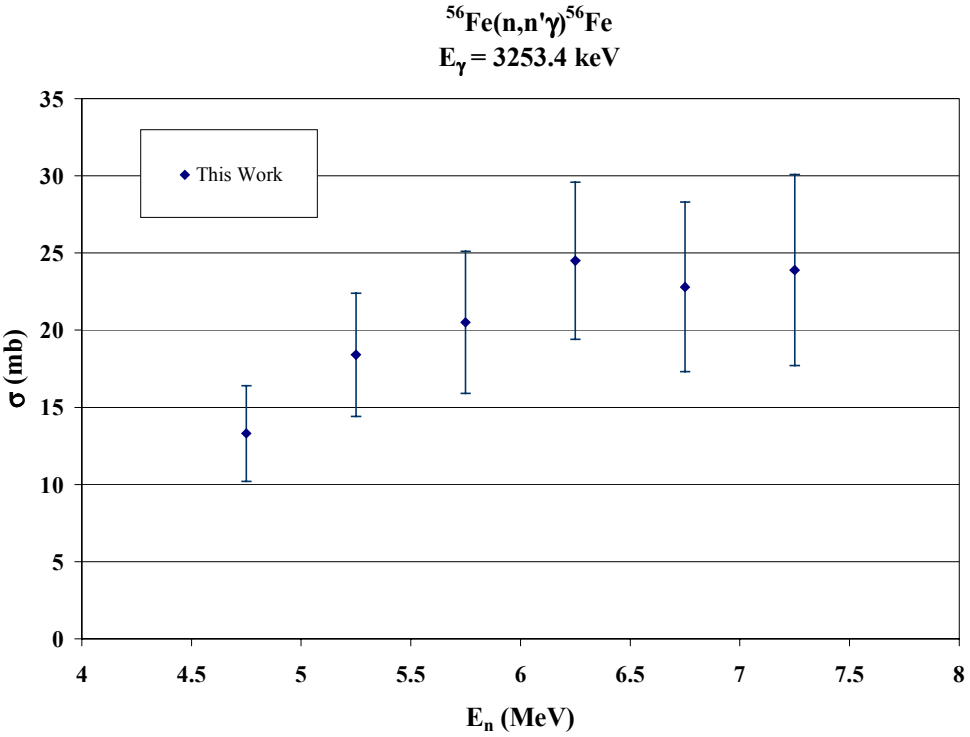

Fig. 33. Cross sections for the 3253.4-keV gamma ray from $^{56}Fe(n,n_{23}'\gamma)$.

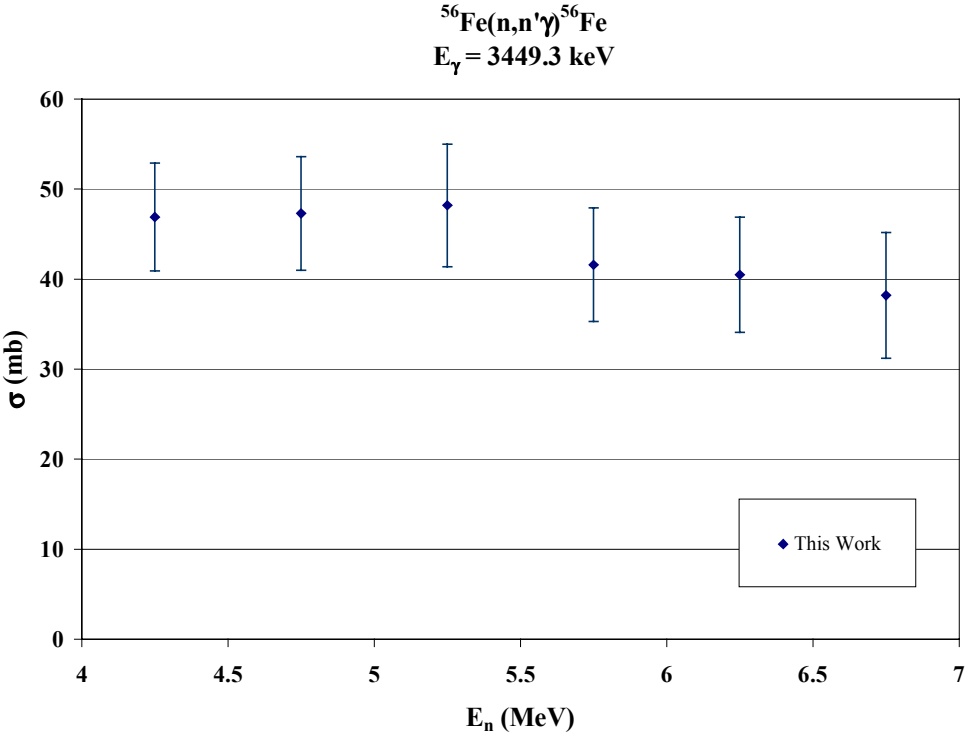

Fig. 34. Cross sections for the 3449.3-keV gamma ray from $^{56}Fe(n,n_{12}'\gamma)$.

Tables

Gamma-Ray Energy Neutron Energy (MeV)	846.8 keV Cross Section (mb)	Error (mb)
1.1	4.86E+02	4.23E+01
1.3	4.18E+02	3.64E+01
1.5	6.12E+02	5.31E+01
1.7	6.01E+02	5.22E+01
1.9	6.38E+02	5.55E+01
2.1	8.13E+02	7.05E+01
2.3	8.17E+02	7.09E+01
2.5	8.77E+02	7.61E+01
2.7	8.69E+02	7.54E+01
2.9	8.91E+02	7.74E+01
3.1	1.04E+03	9.00E+01
3.3	1.01E+03	8.82E+01
3.5	9.53E+02	8.29E+01
3.7	1.05E+03	9.14E+01
3.9	1.03E+03	9.00E+01
4.25	1.04E+03	9.01E+01
4.75	1.07E+03	9.24E+01
5.25	1.16E+03	1.00E+02
5.75	1.13E+03	9.76E+01
6.25	1.05E+03	9.12E+01
6.75	1.08E+03	9.35E+01
7.25	1.14E+03	9.87E+01
7.75	1.10E+03	9.61E+01
8.25	1.07E+03	9.33E+01
8.75	1.07E+03	9.37E+01
9.25	1.08E+03	9.48E+01
9.75	1.08E+03	9.50E+01
10.5	1.07E+03	9.31E+01
11.5	1.07E+03	1.02E+02
12.5	9.11E+02	8.72E+01
13.5	7.93E+02	7.61E+01
14.5	6.63E+02	6.96E+01
15.5	5.34E+02	5.63E+01
16.5	4.16E+02	4.78E+01
17.5	3.50E+02	4.06E+01
18.5	3.08E+02	3.58E+01
19.5	2.22E+02	2.82E+01
22.5	1.75E+02	3.89E+01
27.5	1.10E+02	2.55E+01

Table 2. Cross sections for the production of the 846.8-keV gamma ray.

Gamma-Ray Energy Neutron Energy (MeV)	935.5+931.3 keV Cross Section (mb)	 Error (mb)
13.5	4.13E+01	1.66E+01
14.5	9.58E+01	3.52E+01
15.5	1.16E+02	4.25E+01
16.5	1.58E+02	5.73E+01
17.5	1.57E+02	2.89E+01
18.5	1.71E+02	3.06E+01
19.5	1.68E+02	3.11E+01
22.5	1.58E+02	2.75E+01
27.5	1.20E+02	2.11E+01
32.5	8.02E+01	1.46E+01
37.5	6.16E+01	1.17E+01
42.5	4.87E+01	9.5E+00
47.5	3.99E+01	8.1E+00

Table 3. Cross sections for the production of the 935.5- and 931.3-keV gamma rays. These gamma rays were not analyzed separately.

Gamma-Ray Energy Neutron Energy (MeV)	1037.8 keV Cross Section (mb)	 Error (mb)
3.5	2.06E+01	4.6E+00
3.7	3.42E+01	6.4E+00
3.9	5.19E+01	7.7E+00
4.25	5.14E+01	6.1E+00
4.75	6.38E+01	7.2E+00
5.25	8.89E+01	9.3E+00
5.75	9.58E+01	1.02E+01
6.25	8.62E+01	9.9E+00
6.75	9.23E+01	1.08E+01
7.25	9.14E+01	1.10E+01
7.75	9.47E+01	1.19E+01
8.25	8.46E+01	1.17E+01
8.75	1.00E+02	1.34E+01
9.25	1.04E+02	1.37E+01
9.75	1.02E+02	1.34E+01
10.5	9.73E+01	1.16E+01
11.5	1.09E+02	1.31E+01
12.5	9.89E+01	1.31E+01
13.5	9.20E+01	1.27E+01
14.5	6.44E+01	1.04E+01
15.5	5.22E+01	1.04E+01

Table 4. Cross sections for the production of the 1037.8-keV gamma ray.

Gamma-Ray Energy Neutron Energy (MeV)	1238.3 keV Cross Section (mb)	Error (mb)
2.3	1.75E+01	3.3E+00
2.5	5.33E+01	5.8E+00
2.7	7.00E+01	7.4E+00
2.9	9.36E+01	9.5E+00
3.1	1.24E+02	1.2E+01
3.3	1.46E+02	1.4E+01
3.5	1.50E+02	1.4E+01
3.7	1.81E+02	1.7E+01
3.9	1.74E+02	1.6E+01
4.25	2.16E+02	1.9E+01
4.75	2.71E+02	2.4E+01
5.25	3.23E+02	2.9E+01
5.75	3.57E+02	3.2E+01
6.25	3.50E+02	3.1E+01
6.75	3.89E+02	3.5E+01
7.25	4.21E+02	3.8E+01
7.75	4.60E+02	4.1E+01
8.25	4.29E+02	3.9E+01
8.75	4.37E+02	4.0E+01
9.25	4.66E+02	4.2E+01
9.75	4.52E+02	4.0E+01
10.5	5.04E+02	4.5E+01
11.5	5.21E+02	5.1E+01
12.5	4.90E+02	4.8E+01
13.5	3.88E+02	4.1E+01
14.5	3.05E+02	3.3E+01
15.5	2.80E+02	3.0E+01
16.5	1.76E+02	2.1E+01
17.5	1.49E+02	1.8E+01
18.5	1.26E+02	1.6E+01
19.5	9.20E+01	1.2E+01
22.5	6.31E+01	8.1E+00

Table 5. Cross sections for the production of the 1238.3-keV gamma ray.

Gamma-Ray Energy Neutron Energy (MeV)	1303.4 keV Cross Section (mb)	Error (mb)
6.75	1.92E+01	5.3E+00
7.25	2.52E+01	6.2E+00
7.75	3.40E+01	7.1E+00
8.25	6.92E+01	1.06E+01
8.75	4.41E+01	8.8E+00
9.25	6.10E+01	9.8E+00
9.75	6.65E+01	1.12E+01
10.5	7.83E+01	1.07E+01
11.5	1.01E+02	1.4E+01
12.5	9.58E+01	1.33E+01
13.5	9.06E+01	1.29E+01
14.5	6.69E+01	1.05E+01
15.5	6.67E+01	1.08E+01
16.5	4.26E+01	9.0E+00
17.5	3.25E+01	7.8E+00
18.5	1.56E+01	6.5E+00

Table 6. Cross sections for the production of the 1303.4-keV gamma ray.

Gamma-Ray Energy Neutron Energy (MeV)	1316.4 keV Cross Section (mb)	Error (mb)
14.5	4.85E+01	7.8E+00
15.5	9.23E+01	1.15E+01
16.5	1.27E+02	1.42E+01
17.5	1.52E+02	1.68E+01
18.5	1.97E+02	2.01E+01
19.5	1.79E+02	1.92E+01
22.5	1.84E+02	1.67E+01
27.5	1.30E+02	1.22E+01
32.5	7.81E+01	7.9E+00
37.5	5.10E+01	6.0E+00
42.5	3.79E+01	5.1E+00
47.5	3.18E+01	4.6E+00

Table 7. Cross sections for the production of the 1316.4-keV gamma ray.

Gamma-Ray Energy Neutron Energy (MeV)	1408.1+1408.4 keV Cross Section (mb)	 Error (mb)
1.5	1.52E+01	1.9E+00
1.7	2.51E+01	2.8E+00
1.9	3.76E+01	3.9E+00
2.1	3.79E+01	3.9E+00
2.3	4.18E+01	4.3E+00
2.5	4.23E+01	4.4E+00
2.7	3.68E+01	4.1E+00
2.9	3.87E+01	4.4E+00
3.1	4.39E+01	5.0E+00
3.3	5.43E+01	6.0E+00
3.5	4.56E+01	5.4E+00
3.7	3.90E+01	5.0E+00
3.9	4.67E+01	5.7E+00
4.25	4.13E+01	4.5E+00
4.75	4.29E+01	4.6E+00
5.25	4.51E+01	5.0E+00
5.75	4.20E+01	4.9E+00
6.25	4.46E+01	5.3E+00
6.75	5.21E+01	6.1E+00
7.25	5.16E+01	6.3E+00
7.75	4.63E+01	6.3E+00
8.25	4.45E+01	6.1E+00
8.75		
12.5		
13.5	2.80E+01	5.9E+00
14.5	3.81E+01	6.3E+00
15.5	5.47E+01	7.7E+00
16.5	6.83E+01	1.08E+01
17.5	6.06E+01	1.03E+01
18.5	7.22E+01	1.14E+01
19.5	8.60E+01	1.32E+01
22.5	6.19E+01	8.3E+00
27.5	9.50E+01	1.24E+01
32.5	1.39E+02	1.77E+01
37.5	1.25E+02	2.13E+01
42.5	1.01E+02	1.74E+01
47.5	7.05E+01	1.25E+01
55	5.21E+01	9.1E+00
65	5.01E+01	1.10E+01
75	5.15E+01	1.14E+01
85	3.57E+01	8.1E+00
95	3.92E+01	8.9E+00
150	2.39E+01	5.2E+00

Table 8. Cross sections for the production of the 1408.1- and 1408.4-keV gamma rays, produced by the ^{54}Fe(n,n') and ^{56}Fe(n,3n) reactions.

Gamma-Ray Energy Neutron Energy (MeV)	1434.1 keV Cross Section (mb)	 Error (mb)
19.5	2.93E+01	7.8E+00
22.5	5.03E+01	7.6E+00
27.5	6.94E+01	1.0E+01
32.5	6.00E+01	9.0E+00
37.5	4.22E+01	6.8E+00

Table 9. Cross sections for the production of the 1434.1-keV gamma ray.

Gamma-Ray Energy Neutron Energy (MeV)	1670.8+1668 keV Cross Section (mb)	 Error (mb)
6.75	1.80E+01	5.2E+00
7.25	2.72E+01	6.4E+00
7.75	2.93E+01	6.9E+00
8.25	2.35E+01	6.8E+00
8.75	2.99E+01	7.7E+00
9.25	4.20E+01	8.8E+00
9.75	5.03E+01	1.0E+01
10.50	4.52E+01	7.8E+00
11.50	6.58E+01	9.5E+00
12.50	5.26E+01	9.1E+00
13.50	6.14E+01	9.7E+00
14.50	4.21E+01	8.4E+00
15.50	3.01E+01	7.6E+00

Table 10. Cross sections for the production of the 1670.8- and 1668-keV gamma rays.

Gamma-Ray Energy Neutron Energy (MeV)	1810.8 keV Cross Section (mb)	Error (mb)
2.7	2.22E+01	2.9E+00
2.9	1.01E+02	9.8E+00
3.1	1.70E+02	1.58E+01
3.3	1.62E+02	1.53E+01
3.5	1.68E+02	1.59E+01
3.7	1.71E+02	1.63E+01
3.9	1.38E+02	1.36E+01
4.25	1.40E+02	1.29E+01
4.75	1.26E+02	1.18E+01
5.25	1.39E+02	1.30E+01
5.75	1.25E+02	1.19E+01
6.25	1.21E+02	1.18E+01
6.75	1.23E+02	1.22E+01
7.25	1.33E+02	1.33E+01
7.75	1.20E+02	1.24E+01
8.25	1.05E+02	1.13E+01
8.75	1.02E+02	1.12E+01
9.25	1.09E+02	1.21E+01
9.75	9.95E+01	1.16E+01
10.5	1.08E+02	1.20E+01
11.5	8.34E+01	1.01E+01
12.5	6.95E+01	9.0E+00
13.5	6.23E+01	8.7E+00
14.5	5.08E+01	7.8E+00

Table 11. Cross sections for the production of the 1810.8-keV gamma ray.

Gamma-Ray Energy Neutron Energy (MeV)	2034.8 keV Cross Section (mb)	Error (mb)
4.75	3.04E+01	4.5E+00
5.25	2.53E+01	4.7E+00
5.75	1.78E+01	4.7E+00

Table 12. Cross sections for the production of the 2034.8-keV gamma ray.

Gamma-Ray Energy Neutron Energy (MeV)	2094.9 keV Cross Section (mb)	Error (mb)
3.1	2.55E+01	3.9E+00
3.3	3.39E+01	5.1E+00
3.5	4.49E+01	6.4E+00
3.7	4.10E+01	6.4E+00
3.9	5.15E+01	7.6E+00
4.25	4.25E+01	5.8E+00
4.75	3.60E+01	5.2E+00
5.25	2.37E+01	4.8E+00
5.75	2.60E+01	4.9E+00

Table 13. Cross sections for the production of the 2094.9-keV gamma ray.

Gamma-Ray Energy Neutron Energy (MeV)	2113.1 keV Cross Section (mb)	Error (mb)
3.1	4.51E+01	6.03E+00
3.3	9.20E+01	1.12E+01
3.5	1.06E+02	1.3E+01
3.7	1.14E+02	1.4E+01
3.9	1.15E+02	1.4E+01
4.25	1.10E+02	1.3E+01
4.75	1.09E+02	1.3E+01
5.25	1.05E+02	1.3E+01
5.75	8.05E+01	1.02E+01
6.25	7.33E+01	9.9E+00
6.75	7.26E+01	1.02E+01
7.25	8.64E+01	1.21E+01
7.75	6.14E+01	9.7E+00
8.25	7.66E+01	1.19E+01
8.75	6.48E+01	1.06E+01
9.25	6.57E+01	1.16E+01
9.75	6.61E+01	1.12E+01
10.5	4.95E+01	9.2E+00
11.5	5.18E+01	9.5E+00
12.5	4.08E+01	9.1E+00
13.5	3.92E+01	8.9E+00
14.5	3.06E+01	7.8E+00
15.5	2.59E+01	7.9E+00

Table 14. Cross sections for the production of the 2113.1-keV gamma ray.

Gamma-Ray Energy Neutron Energy (MeV)	2229 keV Cross Section (mb)	Error (mb)
3.9	3.53E+01	5.3E+00
4.25	3.57E+01	4.9E+00
4.75	5.05E+01	6.7E+00
5.25	4.47E+01	6.1E+00
5.75	3.30E+01	5.3E+00
6.25	2.73E+01	5.1E+00
6.75	2.57E+01	5.7E+00

Table 15. Cross sections for the production of the 2229-keV gamma ray.

Gamma-Ray Energy Neutron Energy (MeV)	2273.2 keV Cross Section (mb)	Error (mb)
3.3	4.24E+01	5.3E+00
3.5	6.39E+01	7.1E+00
3.7	6.83E+01	8.2E+00
3.9	6.00E+01	7.6E+00
4.25	6.76E+01	7.2E+00
4.75	6.47E+01	7.1E+00
5.25	4.50E+01	6.1E+00
5.75	3.92E+01	5.8E+00
6.25	3.71E+01	6.1E+00
6.75	3.14E+01	6.7E+00
7.25	3.30E+01	6.7E+00
7.75	2.92E+01	7.0E+00
8.25	2.95E+01	7.0E+00

Table 16. Cross sections for the production of the 2273.2-keV gamma ray.

Gamma-Ray Energy Neutron Energy (MeV)	2522.9 keV Cross Section (mb)	Error (mb)
3.5	1.23E+01	3.30E+00
3.7	5.05E+01	8.57E+00
3.9	6.89E+01	1.14E+01
4.25	6.02E+01	9.47E+00
4.75	6.67E+01	1.06E+01
5.25	7.17E+01	1.17E+01
5.75	7.05E+01	1.15E+01
6.25	5.70E+01	9.56E+00
6.75	4.76E+01	9.13E+00
7.25	4.52E+01	9.35E+00
7.75	4.34E+01	9.33E+00
8.25	4.32E+01	9.52E+00
8.75	4.16E+01	9.76E+00

Table 17. Cross sections for the production of the 2522.9-keV gamma ray.

Gamma-Ray Energy Neutron Energy (MeV)	2985.2 keV Cross Section (mb)	Error (mb)
4.25	2.63E+01	4.2E+00
4.75	2.87E+01	4.7E+00
5.25	3.13E+01	5.5E+00
5.75	2.83E+01	5.5E+00
6.25	2.40E+01	5.4E+00
6.75	2.46E+01	5.8E+00

Table 18. Cross sections for the production of the 2985.2 keV gamma ray.

Gamma-Ray Energy Neutron Energy (MeV)	3202 keV Cross Section (mb)	Error (mb)
4.75	2.51E+01	4.5E+00
5.25	4.79E+01	6.9E+00
5.75	2.02E+01	4.7E+00
6.25	3.64E+01	6.2E+00
6.75	3.73E+01	7.0E+00

Table 19. Cross sections for the production of the 3202-keV gamma ray.

Gamma-Ray Energy Neutron Energy (MeV)	3253.4 keV Cross Section (mb)	Error (mb)
4.75	1.33E+01	3.1E+00
5.25	1.84E+01	4.0E+00
5.75	2.05E+01	4.6E+00
6.25	2.45E+01	5.1E+00
6.75	2.28E+01	5.5E+00
7.25	2.39E+01	6.2E+00

Table 20. Cross sections for the production of the 3253.4-keV gamma ray.

Gamma-Ray Energy Neutron Energy (MeV)	3449.3 keV Cross Section (mb)	Error (mb)
3.7	3.63E+01	5.6E+00
3.9	3.44E+01	5.5E+00
4.25	4.69E+01	6.0E+00
4.75	4.73E+01	6.3E+00
5.25	4.82E+01	6.8E+00
5.75	4.16E+01	6.3E+00
6.25	4.05E+01	6.4E+00
6.75	3.82E+01	7.0E+00

Table 21. Cross sections for the production of the 3449.3-keV gamma ray.